Backman, J., Duncan, R. A., et al., 1988
Proceedings of the Ocean Drilling Program, Initial Reports, Vol. 115

2. EXPLANATORY NOTES[1]

Shipboard Scientific Party[2]

GENERAL INFORMATION

Standard procedures for both drilling operations and preliminary shipboard analysis of the material recovered during Deep Sea Drilling Project (DSDP) and Ocean Drilling Program (ODP) drilling have been regularly amended and upgraded since drilling began in 1968. In this chapter we have assembled information that will help the reader understand the basis for our preliminary conclusions and also help the interested investigator select samples for further analysis. This information applies only to shipboard operations and analyses described in the site reports in the *Initial Reports* of the Leg 115 *Proceedings of the Ocean Drilling Program*. Methods used by various investigators for further shore-based analysis of Leg 115 data will be detailed in the individual scientific contributions published in the *Scientific Results* volume.

AUTHORSHIP OF SITE CHAPTERS

Authorship of the site reports is shared among the entire shipboard scientific party. The Leg 115 site chapters are organized as follows, with authors' names listed alphabetically in parentheses:

Principal Results (Backman, Duncan)
Background and Objectives (Backman, Duncan)
Operations (Hayes)
Lithostratigraphy (Baker, Cullen, Droxler, Peterson, Vilks)
Biostratigraphy (Boersma, Johnson, Mikkelsen, Okada, Rio, Vincent)
Paleomagnetics (Schneider, Vandamme)
Sedimentation Rates (Backman, Boersma, Johnson, Mikkelsen, Okada, Rio, Schneider, Vincent)
Geochemistry (Swart)
Basement Rocks (Baxter, Fisk, Greenough, Hargraves, Tatsumi)
Physical Properties (Hempel, Hurley, Robinson)
Seismic Stratigraphy (Duncan)
Downhole Logging (Hobart)

Data and preliminary interpretations presented in the site chapters reflect knowledge gleaned only from shipboard and initial post-cruise analyses. Results of the more detailed shore-based work presented in the special-studies chapters in the second part of this volume (*Scientific Results*) may in some cases necessitate reinterpretation of these preliminary site chapters.

SURVEY AND DRILLING DATA

The survey data used for specific site selections are discussed in the "Seismic Stratigraphy" section of each site chapter. Short surveys using a precision echo-sounder and seismic profiles were also made on board *JOIDES Resolution* when we approached each site. All geophysical survey data collected during Leg 115 are presented in the "Underway Geophysics" chapter (this volume).

The seismic-profiling system consisted of two 80-in.[3] water guns, a hydrophone array designed at Scripps Institution of Oceanography, Bolt amplifiers, two band-pass filters, and two EDO recorders, usually recording at two different filter settings.

Bathymetric data were displayed on 3.5- and 12-kHz Precision Depth Recorder systems, which consist of sound transceiver, transducer, and recorder. The depths were read on the basis of an assumed 1463 m/s sound velocity. The water depth (in meters) at each site was corrected (1) according to the tables in Matthews (1939) and (2) for the depth of the hull transducer (6.8 m) below sea level. In addition, depths are assumed to be 10.5 m above the water line when referred to the drilling-platform level.

DRILLING CHARACTERISTICS

Because water circulation downhole is open, cuttings are lost onto the seafloor and cannot be examined. The only available information about sedimentary stratification in uncored or unrecovered intervals, other than from seismic data or wireline-logging results, is from an examination of the behavior of the drill string as observed on the drill platform. The harder the layer being drilled, the slower and more difficult it is to penetrate. A number of other factors, however, determine the rate of penetration, so it is not always possible to relate this directly to the hardness of the layers. Bit weight and revolutions per minute, recorded on the drilling recorder, also influence the penetration rate.

DRILLING DEFORMATION

When cores are split, many show signs of significant sediment disturbance. Such disturbance includes the concave-downward appearance of originally horizontal bands, the haphazard mixing of lumps of different lithologies (mainly at the tops of cores), and the near-fluid state of some sediments recovered from tens to hundreds of meters below the seafloor. Core deformation probably occurs during one of three different steps at which the core can suffer stresses sufficient to alter its physical characteristics: cutting, retrieval (with accompanying changes in pressure and temperature), and core handling on deck.

SHIPBOARD SCIENTIFIC PROCEDURES

Numbering of Sites, Holes, Cores, and Samples

Drill sites are numbered consecutively from the first site drilled by *Glomar Challenger* in 1968. A site number refers to one or more holes drilled while the ship was positioned over one acoustic beacon. Multiple holes may be drilled at a single site by pulling the drill pipe above the seafloor (out of one hole), moving the ship some distance from the previous hole, and then drilling another hole.

The first hole drilled at an ODP site is assigned the site number modified by the letter A. Subsequent holes at the same site are designated with the site number modified by letters of the alphabet assigned in chronological sequence of drilling. Note that this differs slightly from the DSDP practice of designating the first hole at a given site by the site number, unmodified, and subsequent holes by the site number modified by letters of the

[1] Backman, J., Duncan, R. A., et al., 1988. *Proc. ODP, Init. Repts.* 115: College Station, TX (Ocean Drilling Program).
[2] Shipboard Scientific Party is as given in the list of Participants preceding the contents.

alphabet. It is important, for sampling purposes, to distinguish among the holes drilled at a site, because recovered sediments or rocks from different holes usually do not come from equivalent positions in the stratigraphic column.

Three varieties of coring systems were employed during Leg 115: (1) the rotary core barrel (RCB) was used for coring basalts and well-lithified sediments, while (2) the advanced piston corer (APC) and (3) the extended core barrel (XCB) were used for coring unlithified or poorly lithified sediments. Cores obtained with the different systems are designated as types "R," "H," and "X," respectively.

The RCB, which is the standard coring device used since DSDP Leg 1, was used with both roller-cone bits and diamond-faced bits. Normally, a core approximately 9.5 m in length is cut and retrieved in each core barrel.

The APC is a modification of the hydraulic piston corer (HPC) originally deployed on DSDP Leg 64. This coring system utilizes an hydraulic piston principle. Fluid is pumped through the drill pipe, activating a piston-driven core barrel which is ejected through the core bit into the sediment at the rate of approximately 6.5 m/s. The extremely high penetration rate is used to decouple the core barrel from the motion of the drill string and to avoid drilling disturbances caused by rotation that normally is encountered in drilling sediments with the RCB. On completion of each coring operation, the core barrel assembly is retrieved by wireline, and the core bit is then "washed" down to the next coring point, where the piston coring procedure is repeated.

The XCB, first deployed on DSDP Leg 90, was developed in order to recover undisturbed cores in the intermediate zone where the sediment is too hard to be piston cored, yet too soft to be recovered effectively with the RCB. It is designed to continue in the same hole, following APC coring, without a bit change. Rotating with the drill string, the XCB employs a diamond-studded cutting shoe that extends 6 in. below the drill bit and that is lubricated by relatively low-energy water jets. This configuration allows the XCB to core soft sediments before they can be washed away by the more energetic drill bit jets. Harder sediments cause the barrel to retract into the drill bit against the pressure of an internal spring, allowing indurated sediments to be cut predominantly by the roller cones and strong water jets of the drill bit.

The cored interval is measured in meters below the seafloor (mbsf). The depth interval assigned to an individual core begins with the depth below the seafloor where the coring operation began and extends to the depth at which the coring operation ended (Fig. 1). For example, each coring interval is usually 9.5 m long, which is the nominal capacity of a core barrel; however, the coring interval may be shorter or longer. "Cored intervals" are not necessarily adjacent to one another but may be separated by "drilled intervals." In soft sediment, the drill string can be "washed ahead" with the core barrel in place (but not recovering sediment) by pumping water down the drill pipe at high pressure to wash the sediment out of the way of the bit and up the space between the drill pipe and wall of the hole. However, if thin hard-rock layers are present, it is possible to get "spotty" sampling of these resistant layers within the washed interval and thus have a cored interval greater than 9.5 m. In drilling hard rock, a center bit may replace the core barrel if it is necessary to drill without core recovery.

Cores taken from a hole are numbered sequentially from the top of the hole downward. Core numbers and their associated cored intervals in meters below the seafloor usually are unique in a given hole. This may not be true, however, if an interval must be cored twice, due to caving of cuttings or other hole problems. Nominally, a fully recovered core consists of 9.3 m of rock or sediment contained in a plastic liner (6.6-cm internal diameter) plus about 0.2 m (without a plastic liner) in the core

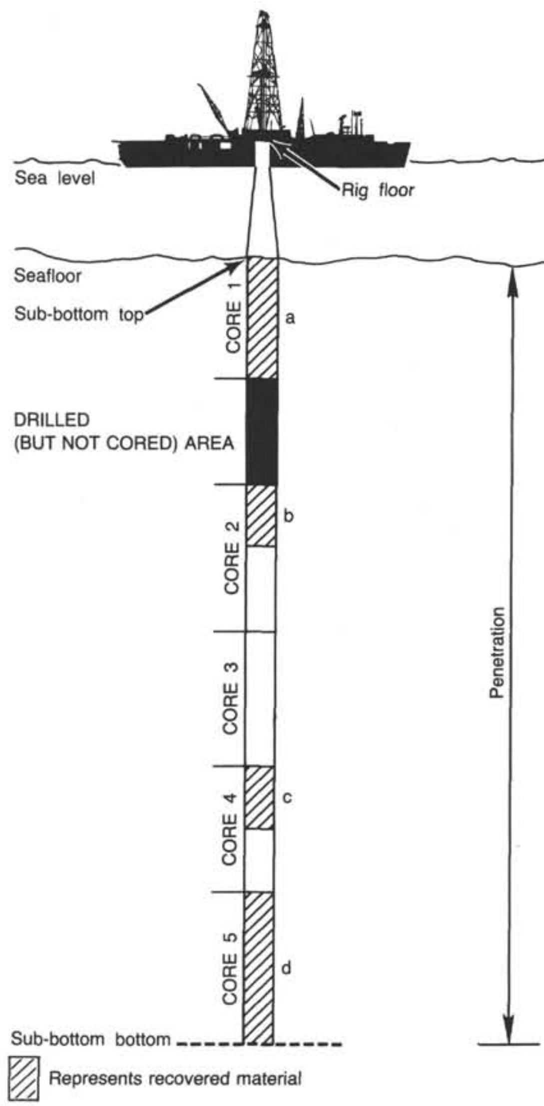

BOTTOM FELT: distance from rig floor to seafloor

TOTAL DEPTH: distance from rig floor to bottom of hole (sub-bottom bottom)

PENETRATION: distance from seafloor to bottom of hole (sub-bottom bottom)

NUMBER OF CORES: total of all cores recorded, including cores with no recovery

TOTAL LENGTH OF CORED SECTION: distance from sub-bottom top to sub-bottom bottom minus drilled (but not cored) areas in between

TOTAL CORE RECOVERED: total from adding a, b, c, and d in diagram

CORE RECOVERY (%): equals TOTAL CORE RECOVERED divided by TOTAL LENGTH OF CORED SECTION times 100

Figure 1. Diagram illustrating terms used in discussing coring operations and core recovery.

catcher. The core catcher is a device at the bottom of the core barrel which prevents the core from sliding out when the barrel is being retrieved from the hole.

Each recovered sediment core is cut into 1.5-m sections which are numbered sequentially from the top of the sediment core (Fig. 2). With full recovery, the sections are numbered from 1 through 7 with the last section possibly being shorter than 1.5 m. With less than full recovery, there will be as many sections as needed to accommodate the length of the core recovered. For example, we would divide 4 m of core into two 1.5-m sections and one 1-m section. If cores are fragmented (recovery less than 100%), sections are numbered sequentially and intervening sections are noted as void, whether shipboard scientists believe that the fragments were contiguous *in situ* or not. Material recovered from the core catcher is placed below the last section when the core is described and labeled core catcher (CC); in sedimentary cores, it is treated as a separate section. Scientists completing visual core descriptions describe each section as a unit.

A recovered basalt core is also cut into 1.5-m sections which are numbered sequentially; however, each piece of rock is then assigned a number (fragments of a single piece are assigned a single number, with individual fragments being identified alphabetically). The core-catcher sample is placed at the bottom of the last section and is treated as part of the last section, rather than separately. Scientists completing visual core descriptions describe each lithologic unit, noting core and section boundaries only as physical reference points.

When, as is usually the case, the recovered core is shorter than the cored interval, the top of the core is equated with the top of the cored interval by convention, in order to achieve consistency in handling analytical data derived from the cores. Samples removed from the cores are designated by distance measured in centimeters from the top of the section to the top and bottom of each sample removed from that section. In curated hard-rock sections, sturdy plastic spacers are placed between pieces which do not fit together in order to protect them from damage in transit and in storage. Therefore, the centimeter interval noted for a basaltic sample has no direct relationship to that sample's depth within the cored interval, but is only a physical reference to the sample's location within the curated core.

A full identification number for a sample consists of the following information: (1) leg, (2) site, (3) hole, (4) core number and type, (5) section number, (6) piece number (for basalts), and (7) interval in centimeters measured from the top of the section. For example, a sample identification of "115-715A-24R-2 (Piece 3B, 30–38 cm)" would represent a sample removed from the interval between 30 and 38 cm below the top of Section 2, Core 24 (R designates that this core was taken with the RCB) of Hole 715A during Leg 115, and that this interval fell within Piece 3, Fragment B, of that section.

Core Handling

As soon as a core was retrieved on deck during Leg 115, a sample was taken from the core catcher and sent to the paleontology laboratory for an initial age assessment.

The core was then placed on the long horizontal rack, and gas samples were taken by piercing the core liner and withdrawing gas into a vacuum-tube sampler. Voids within the core were sought as sites for the gas sampling. The gas samples were analyzed immediately as part of the shipboard safety and pollution prevention program. Next, the core was marked into section lengths, each section was labeled, and the core was cut into 1.5-m sections. Interstitial water (IW) and organic geochemistry (OG) whole-round samples were then taken.

Each section was sealed at the top and bottom by gluing on a color-coded plastic cap: blue to identify the top of a section, and clear for the bottom. A yellow cap was placed on both

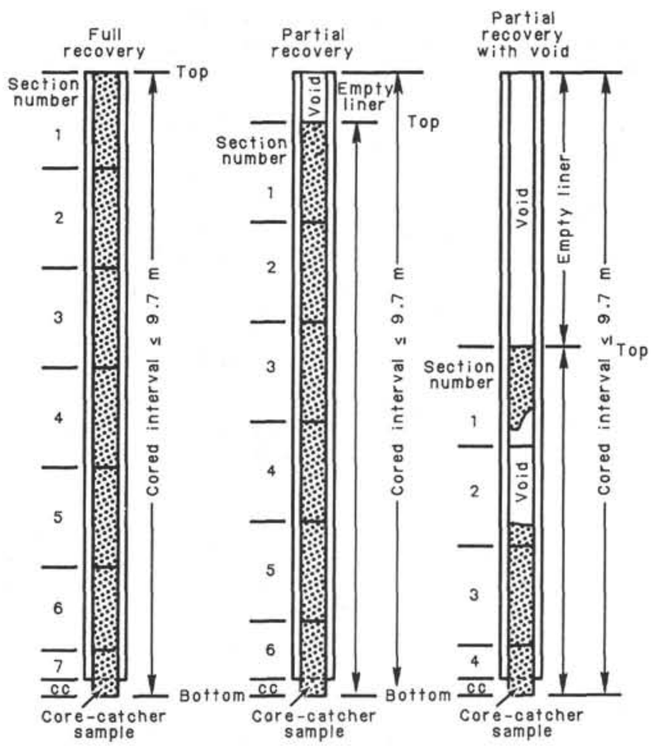

Figure 2. Diagram showing procedure used in cutting and labeling recovered core sections.

section ends from which an IW whole-round sample had been taken. Red end caps were placed on section ends from which an OG sample had been taken. The caps were usually attached to the liner by coating the end of the liner and the inside rim of the end cap with acetone, and then taping the end caps as well to the liner.

Cores were then carried into the laboratory, where the sections were labeled once more using an engraver to mark the full designation of the section. The length of core in each section and the core-catcher sample was measured to the nearest centimeter, and this information was logged into the shipboard core-log database program.

The cores were allowed to warm to room temperature (about 4 hr). After reaching temperature equilibration, whole-round sections were run through the gamma ray attenuation porosity evaluation (GRAPE) device, the *P*-wave logger, the pass-through cryogenic rock magnetometer, and the magnetic susceptibility device (see below). We also completed occasional thermal conductivity measurements.

Cores of relatively soft material were split lengthwise into *working* and *archive* halves. The softer cores were split with a wire or saw, depending on the degree of induration. Harder cores were split with a band saw or diamond saw. Because Leg 115 cores were split with the wire from top to bottom, younger material could possibly have been transported downcore on the split face of each section. Scientists should avoid using the very near-surface part of the split core due to possible contamination.

The *working* half of each core was sampled for both shipboard and shore-based laboratory studies. Each extracted sample was logged with the name of the investigator receiving the sample in the sample computer program. Records of all removed samples are kept by the Curator at ODP headquarters. The extracted samples were sealed in plastic vials or bags and labeled. Samples were routinely taken for shipboard analysis of sonic velocity by the Hamilton Frame method, water content by gravimetric analysis, percentage of calcium carbonate (CO_2 coulometer), and other purposes. Many of these data are reported in the site chapters.

The color, texture, structure, physical disturbance by the drill bit, and composition of each *archive* half were described visually. Smear slides were made from samples taken from the *archive* half and were supplemented by thin sections taken from the *working* half. The *archive* half was then photographed with both black-and-white and color film, a whole core at a time.

Both halves were then put into labeled plastic tubes, sealed, and transferred to cold-storage space aboard the drilling vessel. Leg 115 cores were transferred from the ship by refrigerated vans to cold storage at the Gulf Coast ODP Repository at Texas A&M University, College Station, Texas.

SEDIMENT CORE DESCRIPTION FORMS ("BARREL SHEETS")

The core description forms (Fig. 3), or "barrel sheets," summarize the data obtained during the shipboard analysis of each core. The following discussion explains the ODP conventions used in compiling each part of the core description forms and the exceptions to these procedures adopted by Leg 115 scientists.

Core Designation

Cores are designated using leg, site, hole, and core number and type, as previously discussed (see "Numbering of Sites, Holes, Cores, and Samples" above). In addition, the cored interval is specified in terms of meters below sea level (mbsl) and meters below seafloor (mbsf). On Leg 115, these depths were based on the drill-pipe measurement, as reported by the SEDCO Coring Technician and the ODP Operations Superintendent. Depths when referred to as mbsl were corrected by 10.5 m to account for the height of the drilling platform above the water line.

Age Data

Microfossil abundance, preservation, and zone assignment, as determined by shipboard paleontologists, appear on the core description form under the heading "Biostrat. Zone/Fossil Character." The geologic age determined from the paleontologic and/or paleomagnetic results appears in the "Time-Rock Unit" column. Detailed information on the zonations and terms used to report abundance and preservation appears below (see "Biostratigraphy" section, this chapter).

Paleomagnetic, Physical Properties, and Chemical Data

Because of the large number of samples taken for physical properties and chemical (carbonate) measurements aboard Leg 115, sample locations and data were excluded by design in the columns provided on the core description form. These data, along with the paleomagnetic results and their interpretation, are reported in their entirety in the appropriate sections of each site report. Additional information on shipboard procedures for collecting these types of data appears below (see "Paleomagnetics," "Physical Properties," and "Geochemistry" sections, this chapter).

Graphic Lithology Column

The lithologic classification scheme presented here is represented graphically on the core description forms using the symbols illustrated in Figures 4 and 5. Modifications and additions made to the graphic lithology representation scheme recommended by the JOIDES Sedimentary Petrology and Physical Properties Panel are discussed below (see "Sediment Classification" section, this chapter).

Sediment Disturbance

Recovered rocks, particularly soft sediments, may be slightly to extremely disturbed, and the condition of disturbance is indicated on the core description forms. The symbols for the six disturbance categories used for soft and firm sediments are shown in the "Drilling Disturbance" column in the core description form (Fig. 3). The disturbance categories (Fig. 4) are defined as follows:

1. Slightly disturbed: bedding contacts are slightly bent.
2. Moderately disturbed: bedding contacts have undergone extreme bowing, and firm sediment is fractured.
3. Highly disturbed: bedding is completely disturbed or homogenized by drilling, at some places showing symmetrical diapirlike structure.
4. Soupy: water-saturated intervals have lost all aspects of original bedding.
5. Biscuited: sediment is firm and broken into chunks from 5 to 10 cm long.
6. Brecciated: indurated sediment is broken into angular fragments by the drilling process, perhaps along preexisting fractures.

Sedimentary Structures

The locations and types of sedimentary structures in a core are shown by graphic symbols in the "Sedimentary Structures" column in the core description form (Fig. 3). Figure 4 gives the key for these symbols. It should be noted, however, that distinguishing between natural structures and structures created by the coring process may be extremely difficult.

Color

Colors of the sediment are determined by comparison with the Geological Society of America Rock-Color Chart (Munsell Soil Color Charts, 1971). Colors were determined immediately after the cores were split and while they were still wet.

Lithology

Lithologies are shown in the core description form by one or more of the symbols shown in Figures 5 and 6. The symbols in a group, such as CB1 or SB5, correspond to end-members of sediment compositional range, such as nannofossil ooze or radiolarite. The relative abundances of the sedimentary constituents approximately equal the percentage of the width of the graphic column that its symbol occupies. For example, the left 20% of the column may have a diatom ooze symbol (SB1), whereas the right 80% may have a clay symbol (T1), indicating sediment composed of 80% clay and 20% diatoms. Reference should be made to the lithologic descriptions which accompany each core description form to determine whether sediments consist of simple mixtures or alternating layers of different lithologies.

Samples

The positions of samples taken from each core for shipboard analysis are indicated in the "Samples" column in the core description form. An asterisk (*) indicates the location of smear slide samples, and a pound sign (#) indicates locations where thin sections were cut. The symbols IW and OG designate whole-round interstitial water and frozen organic geochemistry samples, respectively.

Shipboard paleontologists usually base their age determinations on core-catcher samples, although additional samples from other parts of the core may be examined when required.

Lithologic Description—Text

The lithologic description that appears on each core description form consists of two parts: (1) a brief summary of the ma-

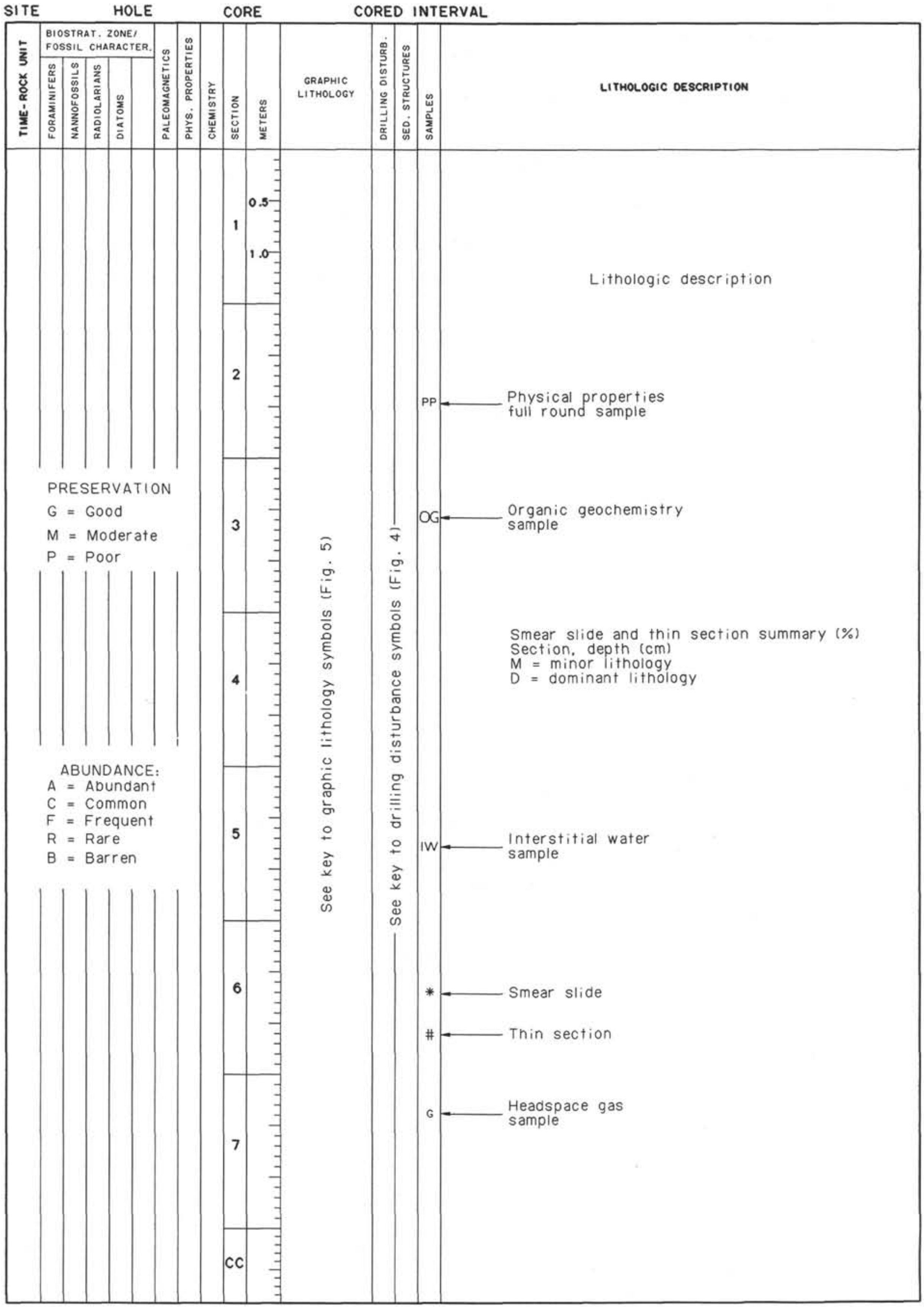

Figure 3. Core description form ("barrel sheet") used for sediments and sedimentary rocks.

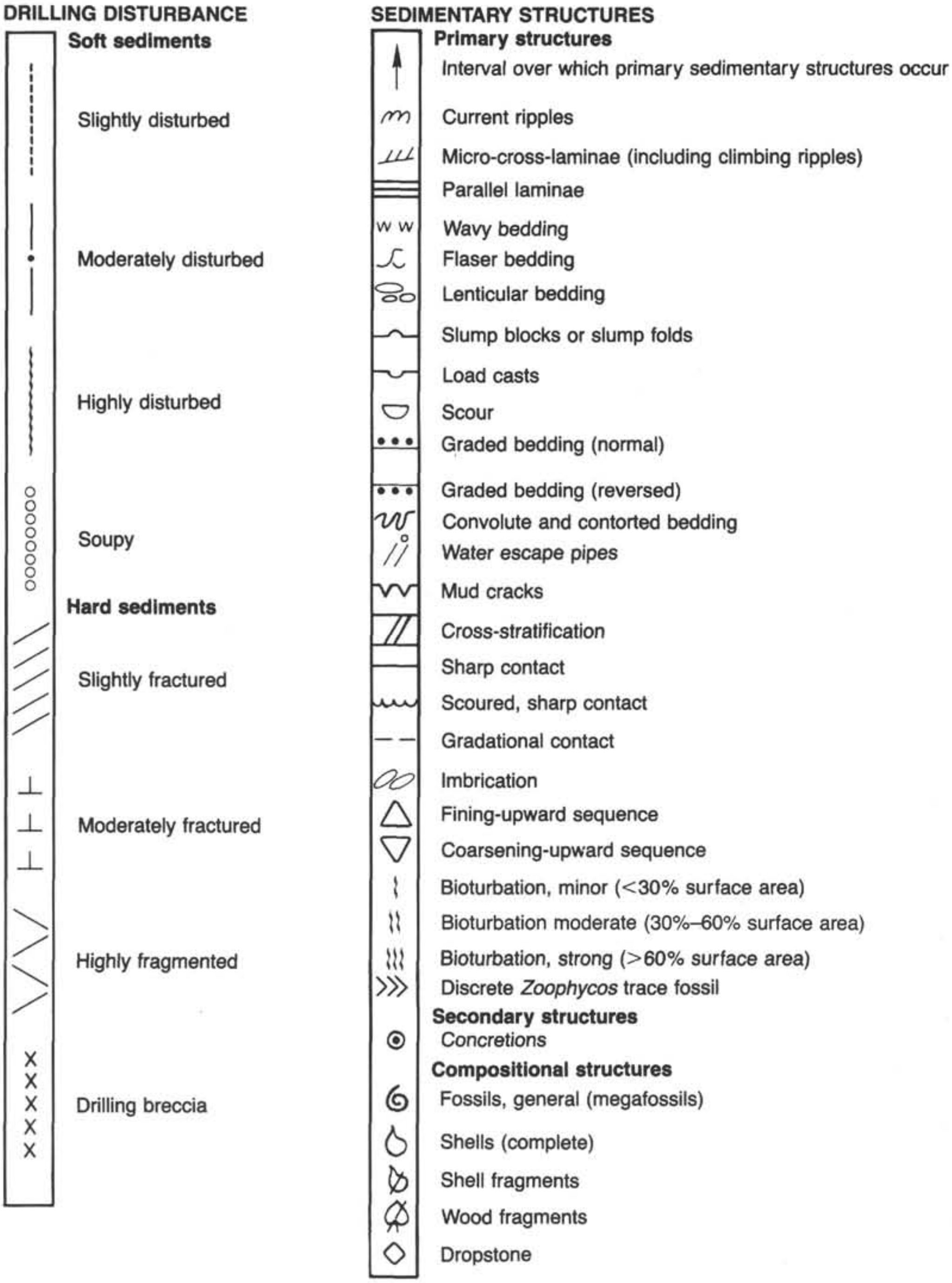

Figure 4. Symbols showing drilling disturbance and sedimentary structures used on Leg 115 core description forms (see Fig. 3).

jor lithologies observed in a given core in order of importance followed by a description of sedimentary structures of features, and (2) a description of minor lithologies observed in the core, including data on color, occurrence in the core, and significant features.

Smear Slide Summary

A table summarizing smear slide and thin-section data, if available, appears on each core description form. The section and interval from which the sample was taken are noted, as well as identification as a dominant (D) or minor (M) lithology in the core. The percentage of all identified components (totaling 100%) is listed. As explained below, these data are used to classify the recovered material.

SEDIMENT CLASSIFICATION

Lithologic Classification of Sediments

The sediment-classification scheme used during Leg 115 is a modified version of the sediment-classification system devised by the Joint Oceanographic Institutions for Deep Earth Sampling (JOIDES) former panel on Sedimentary Petrology and

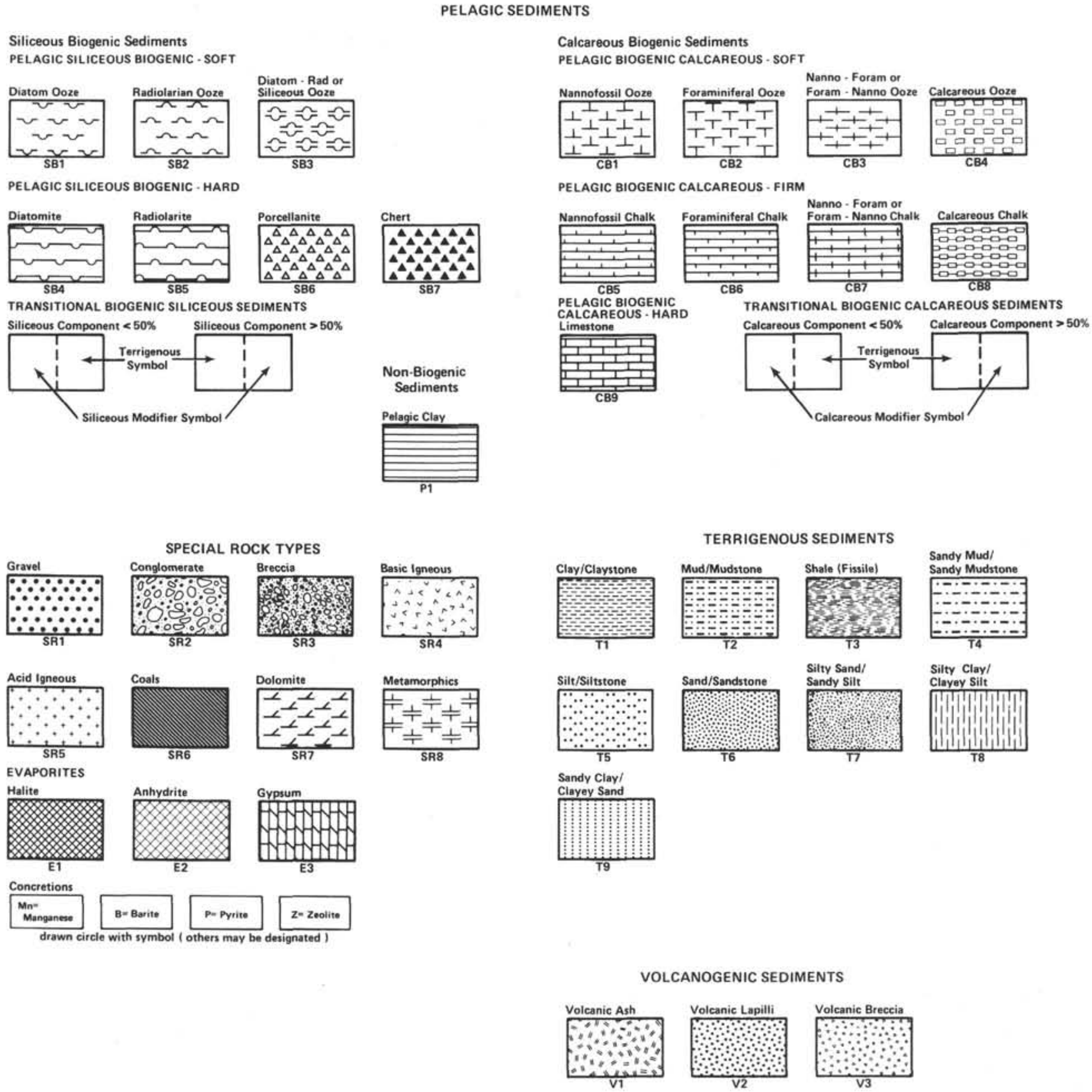

Figure 5. Key to lithologic symbols used in "Graphic Lithology" column on core description form (see Fig. 3).

Physical Properties and adopted for use by the JOIDES Planning Committee in March 1974. The classification scheme used on Leg 115 also incorporates many of the suggestions and terminologies recommended by Dean et al. (1985). This classification scheme is descriptive rather than generic in nature—that is, the basic sediment types are defined on the basis of their texture and composition rather than on the basis of their assumed origin. The texture and composition of sediment samples, and the relative abundances of sedimentary components, were commonly estimated by examining smear slides with a petrographic microscope and thus may differ from more accurate measurements of texture and composition. In some cases, however, the composition of the sediment samples was determined by more accurate shipboard methods, such as by coulometer and X-ray diffraction analyses.

General Rules of Classification

The sediment-classification scheme adopted for Leg 115 differs from the conventional JOIDES sediment-classification scheme in only one major way: the boundary between siliciclastic and biogenic sediment has been shifted from 30% to 50% (Fig. 7). This modification follows the system used by the Leg 108 Scientific Party and classifies samples on the basis of whether the majority of grains are biogenic (either calcareous or siliceous) or siliciclastic in origin.

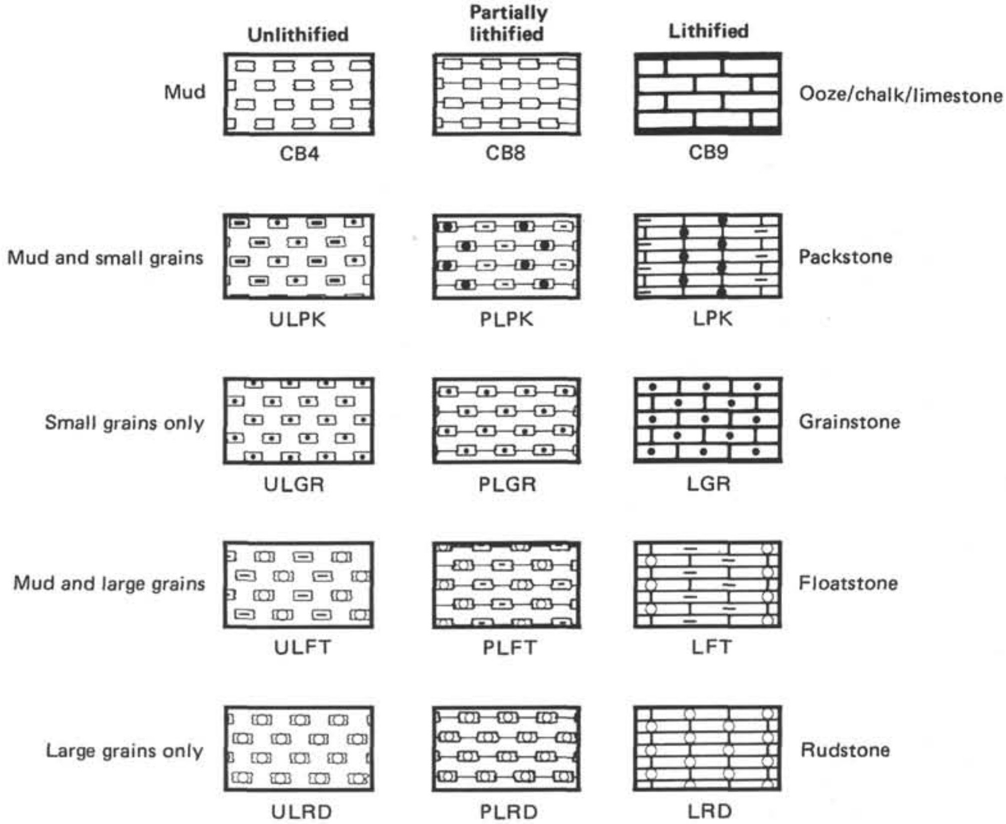

Figure 6. Additional lithologic symbols adapted for use on Leg 115, based on the Dunham (1962) carbonate classification scheme in Figure 8.

Every sediment sample is assigned a main name that defines its sediment type, a major modifier(s) that describes the compositions and/or textures of grains that are present in abundances between 25% and 100%, and a minor modifier(s) that describes the compositions and/or textures of grains that are present in abundances between 10% and 25%. Grains that are present in abundances of less than 10% are considered insignificant and are not included in this classification.

The minor modifiers are always listed first in the string of terms that describes a sample and are attached to the suffix "-bearing," which distinguishes them from major modifiers. When two or more minor modifiers are employed, they are listed in order of increasing abundance. The major modifiers are always listed second in the string of terms that describes a sample and are also listed in order of increasing abundance. The main name is the last term in the string.

The types of main names and modifiers that are employed in this classification scheme differ among the three basic sediment types and are described in the following sections.

Basic Sediment Types

Three basic sediment types are defined on the basis of variations in the relative proportions of calcareous biogenic, siliceous biogenic, and siliciclastic grains: calcareous biogenic sediments, siliceous biogenic sediments, and siliciclastic sediments (Fig. 7).

Calcareous Biogenic Sediments

Calcareous biogenic sediments are composed of less than 50% siliciclastic grains and greater than 50% biogenic grains, but they contain greater proportions of calcareous biogenic grains than siliceous biogenic grains.

The main name of a calcareous biogenic sediment describes its degree of consolidation, using the term *ooze* (soft, unconsolidated), *chalk* (partially to firmly indurated), and *limestone* (hard, consolidated).

The major and minor modifiers for a calcareous biogenic sediment describe the compositions of calcareous biogenic grains as well as the compositions of accessory siliceous biogenic grains and the textures of accessory siliciclastic grains.

The compositions of calcareous biogenic grains are described by the terms *foraminifer*, *nannofossil*, or *calcareous* (for unidentifiable carbonate fragments), followed by the suffix "-bearing" when the grain components are present in minor (10%–25%) amounts. The compositions of siliceous biogenic grains and the textures of siliciclastic grains are described by the terms discussed below.

We also encountered coarse-grained carbonates with highly varied textures on Leg 115. To classify these sediment types adequately, the expanded Dunham (1962) textural classification (Embry and Klovan, 1971) was adopted (Fig. 8). The relative grain-to-mud ratio, grain-vs.-matrix support of the sediment, and grain size were used to adapt the calcareous biogenic categories described above. Ooze, chalk, and limestone remain the fine-grained end-members; coarser lithologies are classified by using the terms "unlithified," "partly lithified," and "lithified," which are used in conjunction with the textural term ("packstone," "grainstone," rudstone," or "floatstone"). Sediments containing sand-sized carbonate grains plus carbonate mud are termed "packstones" (which includes the wackestone category of Dunham, 1962), and sediments with grains only (no mud), "grainstones." Sediments with gravel-sized (and larger) grains plus mud are termed "floatstones," and with grains only (no mud),

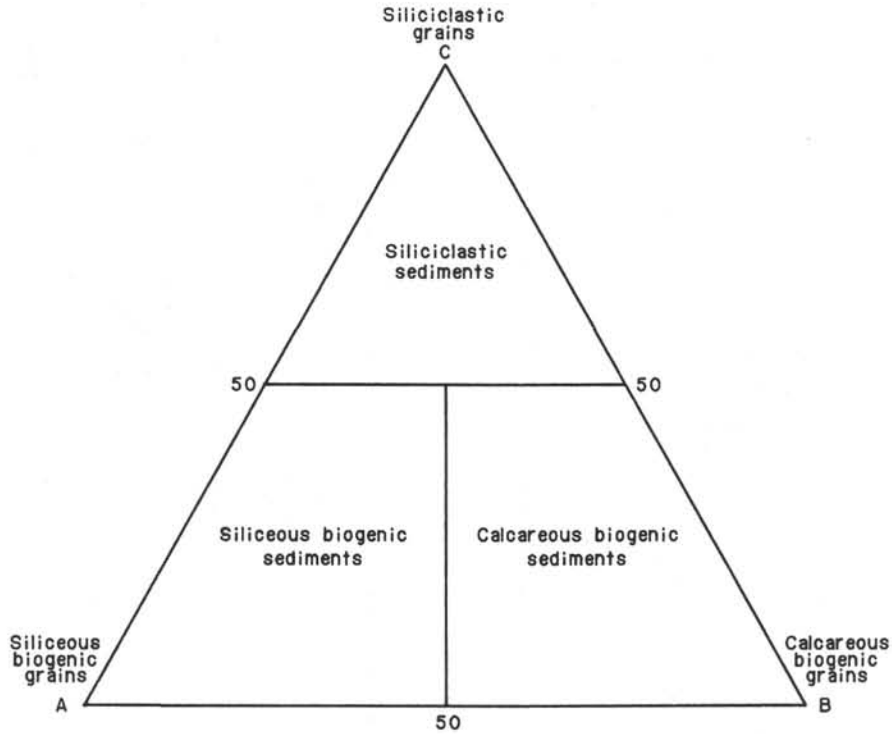

Figure 7. Ternary diagram that defines the three basic sediment types used in the Leg 115 classification scheme on the basis of the relative proportions of siliciclastic, siliceous biogenic, and calcareous biogenic grains.

"rudstones." As seen in Figure 5, the standard ooze, chalk, and limestone symbols are adapted for coarse-grained categories with modifications added to represent mud (a dash), sand-sized grains (a dot), and gravel-sized grains (an open circle).

Siliceous Biogenic Sediments

Siliceous biogenic sediments are composed of less than 50% siliciclastic grains and greater than 50% biogenic grains, but they contain greater proportions of siliceous biogenic grains than calcareous biogenic grains.

The main name of a siliceous biogenic sediment describes its degree of consolidation and/or its composition, using the terms (1) *ooze*: soft, unconsolidated siliceous biogenic sediment; (2) *radiolarite*: hard, consolidated siliceous biogenic sediment composed predominantly of radiolarians; (3) *diatomite*: hard, consolidated siliceous biogenic sediment composed predominantly of diatoms; (4) *porcellanite*: dull, white, porous indurated siliceous biogenic sediment; and (5) *chert*: lustrous, conchoidally fractured, indurated siliceous biogenic sediment.

The major and minor modifiers for a siliceous biogenic sediment describe the compositions of the siliceous biogenic grains, as well as the compositions of accessory calcareous biogenic grains and the textures of accessory siliciclastic grains. The compositions of siliceous biogenic grains can be described by the terms "radiolarian," "diatom," "spicular," and "siliceous" (for unidentifiable siliceous biogenic debris), followed by the suffix "-bearing" when the component is present in minor (10%–25%) amounts. The compositions of accessory calcareous grains are described by those terms discussed above, while the textures of accessory terrigenous grains are described by terms that are discussed in the following section.

Siliciclastic Sediments

Siliciclastic sediments are composed of greater than 50% terrigenous and volcaniclastic grains (i.e, rock and mineral fragments) and less than 50% calcareous and siliceous biogenic grains.

The main name for a siliciclastic sediment describes the textures of the siliciclastic grains and its degree of consolidation. The Wentworth (1922) grain-size scale (Table 1) is used to define the textural-class names for siliciclastic sediments that contain greater amounts of terrigenous grains than volcaniclastic grains. The Wentworth and Williams (1932) grain-size scale (Table 2) is used to define the textural-class names for siliciclastic sediments that contain greater amounts of volcaniclastic grains than terrigenous grains. A single textural-class name (e.g., "sand," "coarse silt," "ash") is used when one textural class is present in abundances in excess of 90%. When two or more textural classes are present in abundances greater than 10%, they are listed in order of increasing abundance (e.g., "silty sand," "ashy clay"). The term *mud* is used to describe mixtures of silt and clay. The hard or consolidated equivalents for the different textural classes are "claystone," "mudstone," "siltstone," and "sandstone."

The major and minor modifiers for a siliciclastic sediment describe the compositions of the siliciclastic grains as well as the compositions of the accessory biogenic grains. The compositions of terrigenous grains can be described by such terms as "quartz," "feldspar," "glauconite," or "lithic" (for rock fragments), and the compositions of volcaniclastic grains can be described by the terms "vitric" (glass), "crystalline," or "lithic." All compositional modifiers are followed by the suffix "-bearing" when the grain component is present in minor (10%–25%) amounts.

Special Rock Types

The definitions and nomenclatures of special rock types not included in the previous section adhere as closely as possible to conventional terminology. Rock types that are included in this category include authigenic minerals (e.g., pyrite, manganese, and zeolite) and evaporites (e.g., halite and anhydrite).

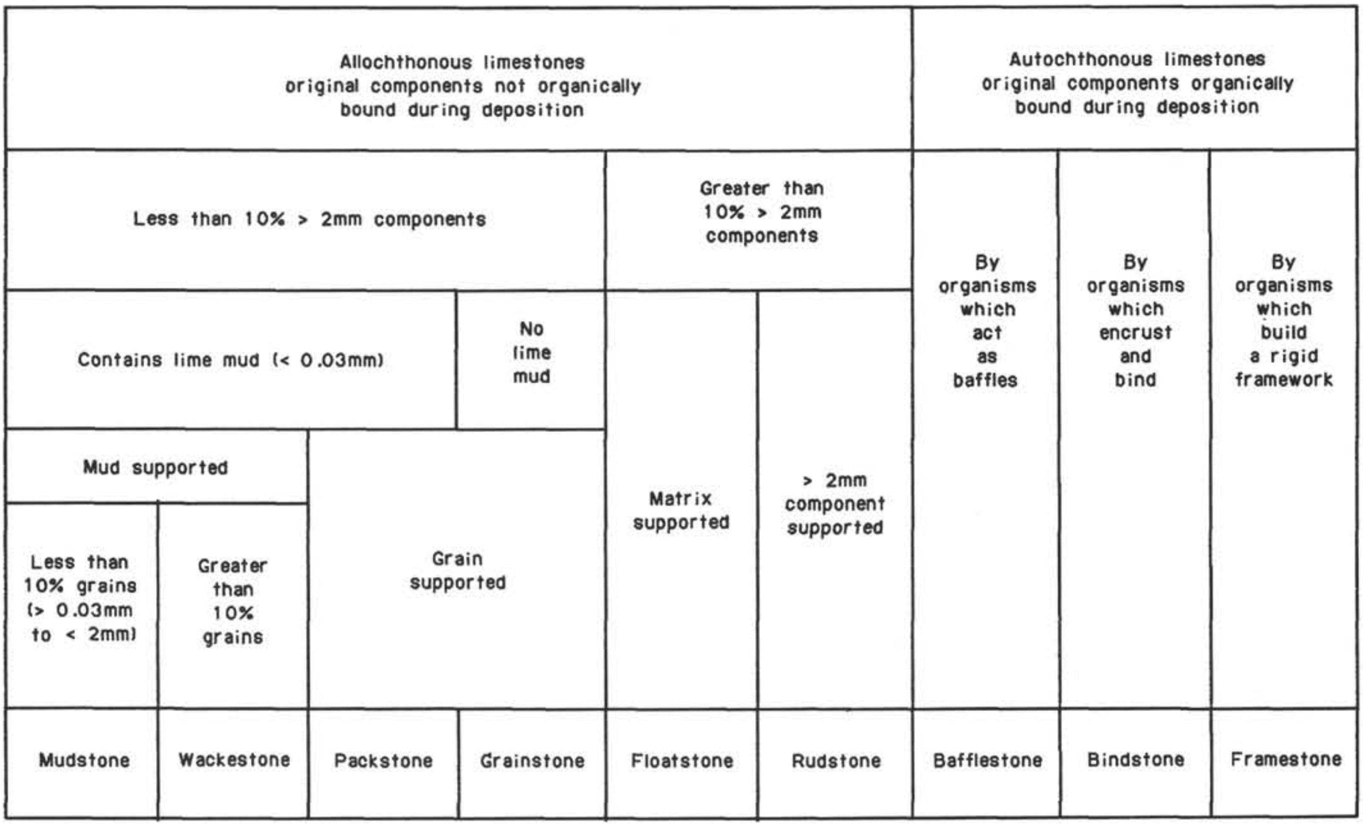

Figure 8. Amplification of the original Dunham (1962) classification of limestones according to depositional texture by Embry and Klovan (1971; Fig. 2), courtesy of the Canadian Society of Petroleum Geologists.

BIOSTRATIGRAPHY

Calcareous Nannofossils

The biostratigraphic schemes proposed by Martini (1971) and Bukry (1973, 1975) are regarded as "standards" for the biostratigraphic classification of Cenozoic marine sediments based on calcareous nannofossils. The Paleogene and the Neogene zones are coded as NP and NN, respectively, in Martini's scheme, which was based on studies of land-section samples as well as deep-sea sediments. Bukry's original scheme, which was modified in 1975, subsequently adopted CP and CN codes for the Paleogene and the Neogene, respectively (Okada and Bukry, 1980). This scheme is based entirely upon studies of low-latitude, deep-sea sediments. However, these two schemes employ the same datum events for many of their boundary definitions and can be easily correlated (e.g., Berggren et al., 1985a, 1985b).

These two zonations already have a fairly good resolution for the Pleistocene, but it seems possible to refine them further. As a matter of fact, Gartner (1977) divided the Pleistocene into seven zones, and further refinements have been suggested by several authors (e.g., Pujos, 1985a, 1985b; Takayama and Sato, 1987; Rio et al., 1988; Matsuoka and Okada, in press). One of the aims for Leg 115 is to examine the possibility of establishing a high-resolution biostratigraphy for the Pleistocene in the Indian Ocean.

For the purpose of biostratigraphic classification of the sedimentary sequences recovered during Leg 115, we make reference to both Martini's and Okada and Bukry's zonal schemes. This allows a better biostratigraphic resolution, within a zonal terminology familiar to most students of deep-sea sediments.

In Table 3 we have listed zonal boundary events from the Paleocene to the Recent for both zonal schemes, together with their proposed ages and some additional events which have proved to be useful, even though they are not used in the "standard" zonations.

The age assignments listed in Table 3 were taken from the quoted literature. We would like to emphasize that the reliability of the listed events and the precision of the estimated ages are not of equal quality. In fact, while most of the Pliocene and Pleistocene events have been directly tied to magnetostratigraphic records through detailed quantitative studies in different areas, most of the pre-Pliocene events have been determined only by presence-absence data. The material drilled during Leg 115 should increase both the reliability and the chronologic precision of the events listed in Table 3, particularly during the pre-Pliocene time interval.

METHODS

Abundance

The abundance of each taxa as a percentage of the total assemblage was defined as follows:

Rare: <0.1% (of the total assemblage).
Few: 0.1%-1.0% (of the total assemblage).
Common: 1.0%-10.0% (of the total assemblage).
Abundant: 10.0%-50.0% (of the total assemblage).
Dominant: >50% (of the total assemblage).

Procedure

The procedure to determine species abundance was as follows:

1. Identify and count the first 100 specimens encountered under a light microscope using 1250× magnification and calculate the percentages.
2. Continue observation until approximately 1,000 nannofossils are scanned. The additional taxa observed during this procedure are generally recorded as few. Taxa which were encountered only once during the

Table 1. Grain-size scale (Wentworth, 1922) for terrigenous grains.

Millimeters		Microns	Phi (φ)	Wentworth size class	
			−20		
	4096		−12	Boulder (−8φ to −12φ)	
	1024		−10		
	256		−8		
				Cobble (−6φ to −8φ)	Gravel
	64		−6		
	16		−4	Pebble (−2φ to −6φ)	
	4		−2		
	3.36		−1.75		
	2.83		−1.5	Granule	
	2.38		−1.25		
	2.00		−1.0		
	1.68		−0.75		
	1.41		−0.5	Very coarse sand	
	1.19		−0.25		
	1.00		0		
	0.84		0.25		
	0.71		0.5	Coarse sand	
	0.59		0.75		
1/2	0.50	500	1.0		
	0.42	420	1.25		
	0.35	350	1.5	Medium sand	Sand
	0.30	300	1.75		
1/4	0.25	250	2.0		
	0.210	210	2.25		
	0.177	177	2.5	Fine sand	
	0.149	149	2.75		
1/8	0.125	125	3.0		
	0.105	105	3.25		
	0.088	88	3.5	Very fine sand	
	0.074	74	3.75		
1/16	0.0625	63	4.0		
	0.053	53	4.25		
	0.044	44	4.5	Coarse silt	
	0.037	37	4.75		
1/32	0.031	31	5.0		
1/64	0.0156	15.6	6.0	Medium silt	
1/128	0.0078	7.8	7.0	Fine silt	
1/256	0.0039	3.9	8.0	Very fine silt	Mud
	0.0020	2.0	9.0		
	0.00098	0.98	10.0	Clay	
	0.00049	0.49	11.0		
	0.00024	0.24	12.0		
	0.00012	0.12	13.0		
	0.00006	0.06	14.0		

Table 2. Grain-size scale (Wentworth and Williams, 1932) for volcaniclastic grains.

Grain size	Unconsolidated	Consolidated
>64 mm	Volcanic rubble	Volcanic breccia
64-4 mm	Volcanic lapilli	Volcanic lapillistone
<4 mm	Volcanic ash	Volcanic tuff

initial count of 100 specimens may be reassigned to the "few" category if fewer than ten individuals are seen during the subsequent scanning.

3. Continue observation until a reasonably large number of nannofossils have been scanned. This number varies depending on the overall abundance of nannofossils, but it is usually more than 10,000 specimens for samples which contain abundant nannofossils.

Preservation

One of our main objectives for Leg 115 was to study the dissolution of calcareous microfossils. Consistent estimates of preservational states, therefore, were important. We followed the criteria developed by Roth and Thierstein (1972), who recognized four states of dissolution and overgrowth:

E-0 and O-0: No sign of dissolution and overgrowth.
E-1 and O-1: Slight dissolution or overgrowth.
E-2 and O-2: Moderate dissolution or overgrowth.
E-3 and O-3: Severe effects of dissolution or overgrowth.

Any combination of "E" and "O" categories can occur, making up 16 different categories. The best preservation is represented by the E-0 O-0 category while the poorest state is expressed as E-3 O-3.

Preparation

Smear slide preparation followed standard procedures: a small piece of sediment is smeared onto a cover glass with a drop of water using a flat toothpick and is dried immediately on a hot plate. The cover glass is then mounted on a glass slide with "Entellan New" cement and degassed on a hot plate to solidify the mounting medium.

Planktonic Foraminifers

Blow's (1969) zonal scheme, which is widely employed for tropical areas, has been successfully applied to Cenozoic foraminiferal sequences recovered in the tropical Indian Ocean (see reviews by McGowran, 1977; Fleischer, 1977; Vincent, 1977). Blow's zonation, slightly modified by Kennett and Srinivasan (1983) for the Neogene, is used here.

Correlations of calcareous plankton biostratigraphic datum events to magnetic polarity stratigraphy have been summarized recently by Berggren et al. (1985a, 1985b) for the Neogene and Paleogene, as well as by Barron et al. (1985a, 1985b) for the Neogene. Ages given by Berggren et al. (1985a) and Barron et al. (1985a, 1985b) for Neogene foraminifer datums are applied (Table 4). For the Paleogene, the biochronology of Berggren et al. (1985b), modified by Nocchi et al. (1986) and Boersma and Premoli Silva (1986) is used.

METHODS

Abundance

Abundance calculations for planktonic species were based on estimates of the following abundance categories: *rare*, <3%; *few*, 3%–15%; *common*, 15%–30%; and *abundant*, >30%. No actual counts were made. Preservational characteristics are divided into three categories: *good*, over 90% of the specimens unbroken; *moderate*, 30%–90% of the specimens showing dissolved or broken chambers; and *poor*, samples dominated by fragments and specimens with broken or dissolved chambers.

Abundance categories for benthic species are as follows: *rare*, <1%; *few*, 1%–5%; *common*, 5%–10%; and *abundant*, >10%. Preservation of benthic foraminifers is determined by the condition of the test and surface chambers. If less than 30% of the specimens examined can be identified because of imperfections, the preservation is considered to be *poor*. If between 30% and 80% of the specimens can be identified, the preservation is considered to be *moderate*. If we could identify more than 80% of the specimens, the preservation is considered to be *good*.

Preparation

Samples for both planktonic and benthic foraminifers were processed by drying thoroughly and then covering with cold water. In most cases, this was sufficient to disaggregate the sample completely; if not, a sample shaker was used. The samples were then washed through a 63-μm sieve, dried under an infrared lamp, and stored. Before examination, the samples were sieved through a 150-μm sieve.

Radiolarians

We believe that the Cenozoic radiolarian zonation derived for the tropical equatorial Pacific will prove satisfactory in the tropical Indian Ocean as well. Sanfilippo et al. (1985) have recently summarized the taxonomy and evolutionary lineages of all stratigraphically important radiolarian taxa commonly found in low-latitude regions of this zonation.

In suggesting tentative "absolute" ages for radiolarian datum levels and zonal boundaries (Table 5), we have followed the schemes of Nigrini (1985) and of Barron et al. (1985b), established on the basis of DSDP Leg 85 sites in the equatorial Pacific. Although much of the material obtained on Leg 85 could not be directly dated paleomagnetically, there were sufficient duplicate sites in which all major microfossil events could be identified, some of which had been correlated to the polarity

Table 3. Species events defining calcareous nannofossil zonal boundaries and their assigned age estimates.

Event	Species	Zone (base)	Age (Ma)	Reference
Increase	*E. huxleyi*	—	0.085	1
FO	*E. huxleyi*	CN15/NN21	0.275	1
LO	*P. lacunosa*	CN14b/NN20	0.460	1
Increase	*G. oceanica*	—	0.90	6
LO	*H. sellii*	—	1.37	2
LO	*C. macintyrei*	—	1.45	2
FO	*G. oceanica*	CN14a	1.6	3
Pliocene/Pleistocene boundary			1.66	3
FO	*G. caribbeanica*	CN13b	1.7	4
LO	*D. brouweri*	CN13a/NN19	1.89	2
LO	*D. triradiatus*	—	1.89	2
Increase	*D. triradiatus*	—	2.07	2
LO	*D. pentaradiatus*	CN12d/NN18	2.35	2
LO	*D. surculus*	CN12c/NN17	2.41	2
LO	*D. tamalis*	CN12b	2.65	2
LO	*Sphenolithus* spp.	CN12a	3.45	2
LO	*R. pseudoumbilica*	CN12a/NN16	3.56	2
Acme base	*D. asymmetricus*	CN11b	?	4
LO	*A. tricorniculatus*	CN11a/NN15	3.7	4
FO	*D. asymmetricus*	NN14	4.1	4
LO	*A. primus*	CN11a	4.4	4
FO	*C. rugosus*	CN10c/NN13	4.6	2
LO	*C. acutus*	CN10c	4.6	2
FO	*C. acutus*	CN10b		
LO	*T. rugosus*	CN10b		
Miocene/Pliocene boundary			4.9	7
LO	*D. quinqueramus*	CN10a/NN12	5.0	8, 9, 10
LO	*A. amplificus*	—	5.6	4
FO	*A. amplificus*	—	5.9	4
FO	*A. primus*	CN9b	6.5	4
FO	*D. quinqueramus*	NN11	8.2	4
FO	*D. berggrenii*	CN9a	8.2	4
FO	*D. neorectus*	CN8b	8.5	4
FO	*D. loeblichii*	CN8b	8.5	4
LO	*D. hamatus*	CN8a/NN10	8.9	4
FO	*C. calyculus*	CN7b	10.0	4
FO	*D. hamatus*	CN7a/NN9	10.0	4
FO	*C. coalitus*	CN6/NN8	10.8	4
LO	*C. floridanus*	CN5b		
FO	*D. kugleri*	CN5b/NN7	11.50	9, 10
LO	*S. heteromorphus*	CN5a/NN6	13.2	11
FO	*C. macintyrei*	CN4	?	
LO	*H. ampliaperta*	NN5	16.0	4
FO	*S. heteromorphus*	CN3	18.6	12, 13
LO	*S. belemnos*	NN4	18.6	12, 13
FO	*S. belemnos*	CN2	20.5	12, 13
LO	*T. carinatus*	NN3	?	
FO	*D. druggii*	CN1c/NN2	23.2	4
Acme top	*C. abisectus*	CN1b	?	
Oligocene/Miocene boundary			23.7	4
LO	*D. bisectus*	CN1a		
LO	*H. recta*	NN1	?	
LO	*S. ciperoensis*	CN1a	25.2	4
LO	*S. distentus*	CP19b/NP25	28.2	4
FO	*S. ciperoensis*	CP19a/NP24	30.2	4
FO	*S. distentus*	CP18	34.2	4
LO	*R. umbilicus*	CP17/NP23	33.8	5
LO	*E. obruta*	—	34.4	5
LO	*C. formosus*	CP16c/NP22	34.9	5
Increase	*E. obruta*	—	36.1	5
Acme top	*E. subdisticha*	CP16b	35.9	4
Eocene/Oligocene boundary			36.2	5
LO	*D. saipanensis*	CP16a/NN21	36.7	5
LO	*D. barbadiensis*	CP16a	37.0	5
FO	*I. recurvus*	CP15b/NP19	37.8	4
FO	*C. oamaruensis*	NP18	39.8	4
LO	*C. grandis*	CP15a	40.0	4
LO	*C. solitus*	CP14b/NP17	42.3	4
LO	*N. fulgens*		45.4	4
FO	*R. umbilica*	CP14a	44.4	5

Table 3 (continued).

Event	Species	Zone (base)	Age (Ma)	Reference
Eocene/Oligocene boundary (cont.)				
LO	*C. gigas*	CP13c	47.0	4
FO	*C. gigas*	CP13b	48.8	4
FO	*N. fulgens*	CP13a/NP15	49.8	4
LO	*D. lodoensis*		50.4	5
FO	*R. inflata*	CP12b	52.0	4
FO	*D. sublodoensis*	CP12a/NP14	52.6	4
LO	*T. orthostylus*	CP11/NP13	53.7	4
FO	*D. lodoensis*	CP10/NP12	55.3	4
LO	*T. contortus*	CP9b/NP11	56.3	4
FO	*T. orthostylus*		56.6	4
FO	*D. diastypus*	CP9a	56.5	4
LO	*Fasciculithus* spp.		57.4	4
Paleocene/Eocene boundary			57.8	4
FO	*C. eodela*	CP8b	58.2	4
FO	*D. multiradiatus*	CP8a	59.1	4
FO	*D. mobilis*	CP7	59.8	4
FO	*D. mohleri*	CP6	60.4	4
FO	*H. kleinpellii*	CP5	61.6	4
FO	*E. tympaniformis*	CP4	62.0	4
FO	*E. macellus*	CP3	63.7	4

Note: FO = first occurrence, LO = last occurrence. All zonal assignments refer to the lower boundary of the zone or subzone. The references refer to the age column and represent (1) Thierstein et al. (1977); (2) Backman and Shackleton (1983), and Backman and Pestiaux (1986); (3) Rio et al. (in press); (4) see data presented by Berggren et al. (1985a, 1985b); (5) Backman (1986); (6) Gartner (1977); (7) Zijderveld et al. (1986); (8) Poore et al. (1983); (9) Lohman (1986); (10) Barton and Bloemendal (1986); (11) Baldauf et al. (1987); (12) Clement and Robinson (1987); and (13) Takayama and Sato (1987).

time scale in nearby piston cores. Thus, we anticipate that the ages of Pacific radiolarian events estimated by Nigrini (1985) and by Barron et al. (1985b) will be a satisfactory working model.

However, we cannot necessarily assume that biostratigraphic datum levels will be globally synchronous. Substantial nonsynchroneity (i.e., on the order of 1 m.y. or greater) has been documented in both latitudinal (Johnson and Nigrini, 1985) and longitudinal (Baldauf et al., 1987) coring transects. Although several datum levels are demonstrably synchronous (e.g., the extinction of *Pseudoemiliania lacunosa*; see Thierstein et al., 1977), our increasing precision in magnetostratigraphic correlation is now allowing us to document and interpret departures from synchroneity.

METHODS

Abundance

Qualitative assessments of the abundance (common, few, rare, absent) and preservation (good, moderate, poor) of radiolarians in each slide were recorded. In assessing the relative abundances of individual taxa, we utilized the following semiquantitative criteria:

Abundant: >20% (of the total assemblage).
Common: 5%–20% (of the total assemblage).
Few: 1%–5% (of the total assemblage).
Rare: 0.1%–1% (of the total assemblage).
Trace: <0.1% (of the total assemblage).
Absent: Not found in an examination of two slides.

Preparation

To obtain clean radiolarian concentrates for microscopic examination, sediments must be disaggregated, sieved to remove the clay-size fraction, and acidified to eliminate the calcareous components. A 5-cm^3 sample was placed in a 400-cm^3 beaker containing 150 mL of a 10% solution of hydrogen peroxide and a small amount of calgon (to aid in disaggregating the sediment). If calcareous components were evident,

Table 4. Species events defining planktonic foraminifer zonal boundaries and their assigned age estimates.

Event	Species	Zonal boundary	Age (Ma)
LO	*Globigerinoides fistulosus*		1.6
FO	*Globigerina calida calida*	N23/N22	?
Pliocene/Pleistocene boundary			
FO	*Globorotalia truncatulinoides*	N22/N21	1.9
LO	*Globoquadrina altispira*		2.9
FO	*Globigerinoides fistulosus*		2.9
LO	*Sphaeroidinellopsis* spp.		3.0
FO	*Globorotalia inflata*		3.0
FO	*Globorotalia tosaensis*	N21/N19	3.1
LO	*Pulleniatina primalis*		3.5
FO	*Sphaeroidinella dehiscens*	N19/N18	5.1
FO	*Globorotalia tumida*	N18/N17	5.2
Miocene/Pliocene boundary			
FO	*Globigerinoides conglobatus*		5.3
LO	*Globoquadrina dehiscens*		5.3
FO	*Pulleniatina primalis*	N17b/N17a	5.8
FO	*Globorotalia plesiotumida*	N17/N16	8.0
FO	*Neogloboquadrina acostaensis*	N16/N15	8.6
LO	*Globorotalia siakensis*	N15/N14	10.4
FO	*Globigerina nepenthes*	N14/N13	11.3
FO	*Sphaeroidinellopsis subdehiscens*	N13/N12	11.8
FO	*Globorotalia fohsi*	N12/N11	13.5
FO	*Globorotalia praefohsi*	N11/N10	14.0
FO	*Globorotalia peripheroacuta*	N10/N9	14.6
FO	*Orbulina suturalis*	N9/N8	15.2
FO	*Praeorbulina sicanus*	N8/N7	16.3
LO	*Catapsydrax dissimilis*	N7/N6	17.6
FO	*Globigerinatella insueta*	N6/N5	17.9
LO	*Globorotalia kugleri*	N5/N4	20.1
FO	*Globorotalia kugleri*	N4/P22	23.7
Oligocene/Miocene boundary			
LO	*Paragloborotalia mendacis*		23.7
FO	*Globigerinoides primordius*		24.5
LO	*Paragloborotalia opima*	P21/P22	28.2
LO	*Streptochilus cubensis*	P21a/P21b	30.0
LO	*Globigerina ampliapertura*	P20/P21	32.8
LO	*Pseudohastigerina*	P19/P20	34.0
Eocene/Oligocene boundary			
LO	hantkeninids, *Globigerinatheka*	P17/P18	36.6
FO	*Globigerina tapuriensis*		36.6
LO	*Turborotalia cerroazulensis* group		36.7
LO	*Globigerinatheka semiinvoluta*		37.6
LO	*Acarinina*	P14/P15	40.6
LO	*Morozovella spinulosa*		41.1
FO	*Globigerinatheka semiinvoluta*		41.3
LO	*Subbotina frontosa*		42.0
LO	*Globigerinatheka beckmanni*	P13/P14	43.0
LO	*Acarinina bullbrooki*		43.0
FO	*Turborotalia pomeroli*		44.7
FO	*Globigerinatheka index*		45.0
FO	*Morozovella lehneri*	P11/P12	46.0
LO	*Morozovella aragonensis*	P11/P12	46.0
FO	*Hantkenina*	P9/P10	52.0
FO	*Morozovella aragonensis*	P7/P8	55.2
FO	*Morozovella formosa*	P6/P7	56.1
Paleocene/Eocene boundary			
LO	*Morozovella velascoensis*		57.8
LO	*Planorotalites pseudomenardii*	P4/P5	58.8
FO	*Planorotalites psuedomenardii*	P3/P4	61.0
FO	*Morozovella velascoensis*		61.7
FO	*Morozovella pusilla*	P3a/P3b	62.0
FO	*Morozovella conicotruncata*	P3a/P3b	62.0
LO	*Morozovella angulata*	P2/P3	62.3

Note: FO = first occurrence, LO = last occurrence. Ages are from Berggren et al. (1985a, 1985b).

they were dissolved by adding hydrochloric acid. The residue was sieved through a 63-μm sieve, and the remaining siliceous microfossils were pipetted evenly onto labeled glass slides. The accompanying water was then evaporated on a hot plate, after which the remaining residue was mounted in a suitable mounting medium (in this instance, Piccolyte), and covered with a 20- by 40-mm cover slip. Two slides were routinely prepared and examined for each sample. We retained the wet residue in the event that reexamination of the material proved to be necessary.

Diatoms

Biostratigraphic studies based on diatoms have accelerated during the last 15 years. Results from these studies have been compiled (Barron, 1985b) into an excellent low-latitude diatom zonation covering the interval from the late Oligocene through Recent time.

The pioneering work on late Cenozoic diatom stratigraphy by Burckle (1972) in the equatorial Pacific was correlated directly to the paleomagnetic stratigraphy. Since then, numerous additional diatom levels have been tied to the magnetostratigraphic record (Burckle, 1977, 1978; Burckle and Opdyke, 1977; Burckle and Trainer, 1979; Burckle et al., 1982). Other low-latitude diatom studies in the Pacific, which has been a key area for diatom biostratigraphic studies since the beginning of the Deep Sea Drilling Project, include those by Bukry and Foster (1973), Schrader (1973), Barron (1980, 1983, 1985a, 1985b), Sancetta (1983), Barron et al. (1985a), and Baldauf (1985a). Schrader (1974) proposed a low-latitude diatom zonation for the late Miocene to Quaternary of the Indian Ocean, and Jouse and Kazarina (1974) reported on Pleistocene diatoms from Site 262 in the eastern Indian Ocean.

The diatom zonation used during Leg 115 is that compiled by Barron (1985a, 1985b). It consists of Burckle's (1972) late Miocene through Quaternary zonation; Barron's (1983) late Oligocene to middle Miocene zonation; and Fenner's (1985) Paleogene zonation.

The marine magnetic anomaly time scale used during Leg 115 is that of Berggren et al. (1985a, 1985b). This time scale, however, does not incorporate a diatom zonation. Magnetostratigraphically calibrated first (FO) and last (LO) occurrences of diatom species are based, therefore, on the information given in Barron (1985a, 1985b) and Barron et al. (1985a, 1985b). The species events and their assigned age estimates are listed in Table 6. The majority of the younger events have a direct paleomagnetic control, whereas the ages of most of the older events often lack magnetostratigraphic control.

METHODS

Abundance

The method for tabulating diatom abundance followed Baldauf (Shipboard Scientific Party, 1988) and is given as follows:

A: Two or more valves per 1 field of view.
C: One diatom valve per 1 field of view.
F: One diatom valve per 2 fields of view.
R: One diatom valve per 4 fields of view.
VR: One diatom valve per 8 fields of view.
O (barren): No diatoms.

Preservation

Criteria for assessing diatom preservation also followed Baldauf (Shipboard Scientific Party, 1988) and are given as follows:

Good: More than 95% of all diatom valves whole, and no sign of partial dissolution.

Moderate: 30%–95% of all valves whole; moderate breakage and slight dissolution; some fragile specimens still complete.

Poor: Less than 30% of all valves whole; extensive breakage; partial dissolution; delicate structures not present on valves.

Table 5. Tropical Cenozoic radiolarian zonation and diagnostic datum levels, modified after Sanfilippo et al. (1985). Estimated ages of datum levels are from Barron et al. (1985b) and Nigrini (1985).

Zone	Approximate age	Top or bottom	Species
	0		
B. invaginata			
	0.17	B	*Buccinosphaera invaginata*
C. tuberosa	0.42	T	*Stylatractus universus*
	0.45	B	*Collosphaera tuberosa*
A. ypsilon	0.70	T	*Pterocorys campanula*
	0.74	T	*Anthocyrtidium nosicaae*
	0.77	B	*Pterocorys hertwigii*
	0.85	B	*Antocyrtidium euryclathrum*
	1.00	T	*Anthocyrtidium angulare*
A. angulare	1.15	B	*Lamprocyrtis nigriniae*
	1.15	T	*Lamprocyrtis neoheteroporus*
	1.50	T	*Anthocyrtidium michelinae*
	1.55	T	*Pterocanium prismatium*
P. prismatium	1.60	B	*Anthocyrtidium angulare*
	1.85	T	*Theocorythium vetulum*
	2.35	T	*Anthocyrtidium jenghisi*
	2.47	B	*Pterocorys sabae*
	2.5	B	*Theocorythium trachelium*
	2.6	T	*Stichocorys peregrina*
S. pentas	3.27	T	*Phormostichoartus fistula*
	3.35	T	*Lychnodictyum audax*
	3.53	T	*Phormostichoartus doliolum*
	3.78	B	*Amphirhopalum ypsilon*
	3.80	T	*Spongaster pentas*
	3.80	B	*Spongaster tetras*
	3.88	T	*Anthocyrtidium prolatum*
	4.3	T	*Solenosphaera omnitubus*
	4.45		*S. berminghami* → *S. pentas*
S. peregrina	4.6	B	*Pterocanium prismatium*
	5.5	T	*Acrobotrys tritubus*
	?	T	*Calocycletta caepa*
	?	T	*Siphostichartus corona*
	6.4		*S. delmontensis* → *S. peregrina*
D. penultima	6.8	B	*Solenosphaera omnitubus*
	6.9		*D. antepenultima* → *D. penultima*
	7.0	T	*Diartus hughesi*
D. antepenultima		B	*Spongaster berminghami*
		T	*Dictyocoyne ontongensis*
	7.6	B	*Acrobotrys tritubus*
		T	*Botryostrobus miralestensis*
	8.6		*D. petterssoni* → *D. hughesi*
D. petterssoni			*D. laticonus* → *D. antepenultima*
			L. neotera → *L. bacca*
		T	*Cyrtocapsella japonica*
		T	*Lithopera thornburgi*
	11.4	T	*Cyrtocapsella tetrapera*
	11.4	T	*Cyrtocapsella cornuta*
		T	*Carpocanopsis cristata*
		B	*Phormostichoartus doliolum*
		T	*Dorcadospyris alata*
		T	*Stichocorys wolffii*
		B	*Cyrtocapsella japonica*
	11.5	B	*Diartus petterssoni*
D. alata			*L. renzae* → *L. neotera*
		B	*Lithopera thornburgi*
		B	*Phormostichoartus corbula*
		T	*Dorcadospyris alata*
		T	*Calocycletta virginis*
		T	*Carpocanopsis bramlettei*
		T	*Calocycletta costata*
		T	*Didymocyrtis violina*
		T	*Didymocyrtis tubaria*
		B	*Lithopera renzae*
		T	*Docadospyris forcipata*
	15.3		*D. dentata* → *D. alata*
C. costata		T	*Eucyrtidium diaphanes*
		T	*Carpocanopsis cingulata*
		B	*Siphostichartus corona*
	16.2	T	*Didymocyrtis prismatica*
		B	*Carpocanopsis cristata*
		T	*Carpocanopsis favosa*
	16.5	T	*Lychnocanoma elongata*
	17.3	B	*Calocycletta costata*
S. wolffii	17.3	B	*Dorcadospyris dentata*
		B	*Calocycletta caepa*

Table 5 (Continued).

Zone	Approximate age	Top or bottom	Species
————	18.2	B	*Stichocorys wolffii* ————
		T	*Dorcadospyris ateuchus*
	20.3	B	*Didymocyrtis tubaria*
S. delmontensis		B	*Didymocyrtis violina*
	21.1	B	*Stichocorys delmontensis*
————	21.3	T	*Theocyrtis annosa* ————
		B	*Carpocanopsis bramlettei*
		T	*Calocycletta serrata*
	21.5	B	*Calocycletta virginis*
C. tetrapera	21.9		*C. pegetrum* → *C. leptetrum*
		B	*Botryostrobus miralestensis*
		B	*Carpocanopsis cingulata*
————	22.1	B	*Cyrtocapsella tetrapera* ————
	22.1	B	*Cyrtocapsella cornuta*
		B	*Carpocanopsis favosa*
L. elongata		B	*Calocycletta serrata*
	22.6	T	*Artophormis gracilis*
	22.6	T	*Dorcadospyris papilio*
————	24.1	B	*Lychnocanoma elongata* ————
		B	*Carpocanopsis cingulata*
		B	*Dorcadospyris forcipata*
		T	*Lithocyclia angusta*
D. ateuchus		B	*Dorcadospyris papilio*
		B	*Theocyrtis annosa*
		T	*Lithocyclia crux*
		T	*Theocyrtis tuberosa*
————	33.0		*T. triceros* → *D. ateuchus* ————
		B	*Didymocyrtis prismatica*
		B	*Lychnodictyum audax*
T. tuberosa			*A. barbadensis* → *A. gracilis*
		T	*Dictyoprora mongolfieri*
		B	*Lithocyclia crux*
————	36.0		*L. aristotelis* → *L. angusta* ————
		T	*Calocylas turris*
		T	*Lychnocanoma bandyca*
		T	*Thyrsocyrtis bromia*
		T	*Thyrsocyrtis lochites*
		T	*Thyrsocyrtis tetracantha*
T. bromia		T	*Thyrsocyrtis triacantha*
		T	*Carpocanistrum azyx*
		T	*Eusyringium fistuligerum*
		T	*Podocyrtis goetheana*
		B	*Lychnocanoma bandyca*
		T	*Podocyrtis chalara*
		B	*Calocyclas turris*
————	41.0	B	*Carpocanistrum azyx* ————
		B	*Thyrsocyrtis bromia*
		B	*Thyrsocyrtis tetracantha*
P. goetheana		T	*Theocotylissa ficus*
		T	*Sethochytris triconiscus*
			L. ocellus → *L. aristotelis*
————	42.0	B	*Podocyrtis goetheana* ————
		T	*Podocyrtis trachodes*
P. chalara		T	*Phormocyrtis striata striata*
		B	*Tristylospyris triceros*
————	43.0		*P. mitra* → *P. chalara* ————
		B	*Cryptoprora ornata*
		T	*Podocyrtis ampla*
		T	*Eusyringium lagena*
P. mitra		B	*Artophormis barbadensis*
		B	*Thyrsocyrtis lochites*
		B	*Sethochytris triconiscus*
		T	*Podocyrtis fasciolata*
————	45.0		*P. sinuosa* → *P. mitra* ————
		B	*Podocyrtis trachodes*
			E. lagena → *E. fistuligerum*
P. ampla		T	*Podocyrtis dorus*
		B	*Podocyrtis fasciolata*
		T	*Theocotyle venezuelensis*
————	46.5		*P. phyxis* → *P. ampla* ————
		T	*Theocotyle nigriniae*
		T	*Theocotyle conica*
			P. diamesa → *P. phyxis*
T. triacantha		T	*Theocorys anaclasta*
		T	*Thyrsocyrtis hirsuta*
		T	*Thyrsocyrtis robusta*
			T. tensa → *T. triacantha*
————	48.0	B	*Eusyringium lagena* ————

Table 5 (Continued).

Zone	Approximate age	Top or bottom	Species
D. mongolfieri		B	*Podocyrtis dorus*
			T. cryptocephala → *T. conica*
		T	*Calocycloma castum*
	49.0	B	*Dictyoprora mongolfieri*
T. cryptocephala			*P. aphorma* → *P. sinuosa*
		B	*Thyrsocyrtis robusta*
		B	*Theocotyle venezuelensis*
		T	*Buryella clinata*
	50.0		*T. nigriniae* → *T. cryptocephala*
P. striata striata		T	*Podocyrtis platypus*
		T	*Lamptonium sanfilippoae*
		B	*Thyrsocyrtis rhizodon*
		B	*Podocyrtis platypus*
		B	*Podocyrtis diamesa*
		B	*Podocyrtis aphorma*
			Phormocyrtis striata exquisita → *P. striata striata*
	51.0	B	*Theocorys anaclasta*
B. clinata		T	*Theocotylissa fimbria*
		T	*Pterocodon ampla*
		T	*Bekoma bidartensis*
		T	*Buryella tetradica*
		T	*Thyrsocyrtis tarsipes*
		B	*Lithocyclia ocellus*
		B	*Thyrsocyrtis tensa*
			T. alpha → *T. ficus*
		B	*Lamptonium sanfilippoae*
		B	*Theocotyle nigriniae*
		B	*Thyrsocyrtis hirsuta*
	52.5		*P. anteclinata* → *B. clinata*
B. bidartensis		B	*Theocotylissa fimbria*
			T. auctor → *T. alpha*
		B	*Calocycloma castum*
			Lamptonium pennatum → *L. fabaeforme fabaeforme*
	55.5	B	*Bekoma bidartensis*

Barren: No diatoms.

Preparation

Shipboard sample preparation followed the method described in Baldauf (1985b) in part. A 1-cm^3 sample was placed in a 250-mL beaker, and 10% HCl was added until the carbonate reaction ceased. We gently heated the sample until the liquid became light yellow in color and then added 200-mL distilled water. The sample was decanted after 1½ hours of settling. This process was repeated three times. Strewn slides of acid-cleaned material were prepared on 22- by 40-mm cover slips and mounted on 25- by 75-mm glass slides using Hyrax mounting medium.

Procedure

The diatom slides were examined with a Zeiss compound microscope. At least 450 fields of view were examined at 500× magnification; verification of individual species was made at 1250× when necessary. The criteria for distinguishing whole from broken diatoms followed Schrader and Gersonde (1978).

PALEOMAGNETICS

Magnetostratigraphy

Prior to drilling, we conducted various calibration experiments to establish the accuracy of the basic measurement apparatus and to check the operation of the processing software. After drilling commenced, we performed measurements on core sections in a more or less routine fashion, with our procedures changing slightly through the course of the cruise. Initially, we employed the multishot orientation tool in an effort to orient the APC cores; however, the results appeared to be unreliable and we later abandoned its use. Therefore, any declinations quoted are in core coordinates only (i.e., measured with respect to the double line on the core liner).

Measurements with the pass-through cryogenic magnetometer often proved to be uninterpretable because of physical disturbance (such as twisting in XCB cores), rust contamination, or simply low signal levels. In addition, many of the sediments were affected by a pervasive remagnetization associated with the core barrels. This remagnetization effect is discussed in detail in the "Paleomagnetics" discussion in the "Site 709" chapter. In other site chapters, we comment on those problems which apply, but otherwise we include in the discussion of paleomagnetics only those results which appear to reflect primary magnetizations.

In addition to the pass-through measurements, discrete sampling was undertaken following the usual methods: soft sediments were sampled by pressing plastic sample boxes into the cores; more indurated sediments were sampled by sawing out small cubes. From the basement rocks recovered, oriented "minicore" samples were obtained using a standard 2.5-cm diamond drill. Routine sampling was conducted as follows: (a) in soft sediments, one discrete sample was taken in each 1.5-m core section; and (b) in basement rocks, one minicore was taken from each 1.5-m section, or from individual petrologic units where these are less than 1.5 m thick.

To estimate the maximum likelihood mean of the inclination-only data obtained, we used the technique of McFadden and Reid (1982). From this algorithm we determined the mean and the Fisher precision parameter, kappa (κ). The alpha 95 values were calculated using standard Fisher statistics. Paleolatitude was calculated from the dipole formula with the quoted error equal to dp of the virtual geomagnetic pole.

Whenever possible, we have offered in the site chapters an interpretation of the magnetic polarity stratigraphy using the mag-

Table 6. Species events defining diatom zonal boundaries and their assigned age estimates.

Event	Species	Zone (base)	Age (Ma)	Magnetic
LO	*Nitzschia reinholdii*	(*P. doliolus*)	0.65	x
LO	*Rhizosolenia matuyamai*		0.93	x
FO	*Rhizosolenia matuyamai*		1.00	x
LO	*Rhizosolenia praebergonii* var. *robustus*	(B subzone–*N. reinholdii*)	1.60	x
Pliocene/Pleistocene boundary			1.66	
FO	*Pseudoeunotia doliolus*	(*N. reinholdii*)	1.80	x
LO	*Rhizosolenia praebergonii*		1.82	x
LO	*Thalassiosira convexa* var. *convexa*	(C. subzone–*R. praebergonii*)	2.1	x
LO	*Nitzschia jouseae*	(B subzone–*R. praebergonii*)	2.6	x
FO	*Rhizosolenia praebergonii*	(*R. praebergonii*)	3.0	x
LO	*Actinocyclus ellipticus* f. *lanceolata*		3.5	
FO	*Thalassiosira convexa* var. *convexa*		3.6	x
FO	*Asteromphalus elegans*		3.9	x
LO	*Nitzschia cylindrica*		4.3	x
FO	*Nitzschia jouseae*	(*N. jouseae*)	4.5	x
LO	*Thalassiosira miocenica*	(C. subzone–*T. convexa*)	5.1	x
FO	*Thalassiosira oestrupii*		5.1	x
Miocene/Pliocene boundary			5.3	
LO	*Asterolampra acutiloba*		5.35	x
LO	*Nitzschia miocenica*		5.6	x
LO	*Thalassiosira praeconvexa*	(B. subzone–*T. convexa*)	5.8	x
FO	*Thalassiosira convexa* var. *aspinosa*	(*T. convexa*)	6.1	x
FO	*Thalassiosira miocenica*		6.1	x
FO	*Thalassiosira praeconvexa*	(B subzone–*N. miocenica*)	6.3	x
LO	*Nitzschia porteri*		6.7	x
FO	*Nitzschia miocenica*	(*N. miocenica*)	6.8	x
LO	*Rossiella paleacea*		6.9	x
LO	*Thalassiosira burckliana*	(B subzone–*N. porteri*)	7.0	x
LO	*Coscinodiscus yabei* (= LO *C. plicatus*)	(*N. porteri*)	7.5	x
FO	*Nitzschia reinholdii*		8.0	
FP	*Thalassiosira burckliana*	(B subzone–*C. yabei*)	8.0	x
LO	*Coscinodiscus temperei* var. *delicata*		8.2	
LO	*C. vetustissimus* var. *javanica*		8.5	x
FO	*C. vetustissimus* var. *javanica*		8.8	x
LO	*Denticulopsis hustedtii* (tropical range)		8.8	
LO	*Actinocyclus moronensis*	(*C. yabei*)	8.9	x
FO	*Nitzschia fossilis*		9.8	
LO	*Coscinodiscus tuberculatus*		10.4	x
LO	*Denticulopsis punctata* f. *hustedtii*		10.7	x
LO	*Craspedodiscus coscinodiscus*	(*A. moronensis*)	10.7	
FO	*Hemidiscus cuneiformis*		11.2	x
FO	*Coscinodiscus temperei*	(*C. coscinodiscus*)	11.8	x
LO	*Denticulopsis nicobarica*		12.6	
LO	*Actinocyclus ingens* (tropical range)		12.8	
LO	*Coscinodiscus lewisianus*	(*C. gigas* var. *diorama*)	12.9	
FO	*Denticulopsis hustedtii* (main tropical range)		13.7	
LO	*Cestodiscus peplum*	(*C. lewisianus*)	14.1	x
FO	*Coscinodiscus blysmos*		14.4	
LO	*Annellus californicus*	(B subzone–(*C. peplum*)	15.0	x
LO	*Coscinodiscus praenodulifer*		15.5	
FO	*Actinocyclus ingens* (tropical range)		15.5	
LO	*Coscinodiscus lewisianus* var. *similis*		15.7	

Table 6 (Continued).

Event	Species	Zone (base)	Age (Ma)	Magnetic
LO	*Thalassiosira fraga*		16.3	
FO	*Cestodiscus peplum*	(*C. peplum*)	16.4	x
LO	*Synedra miocenica*		16.5	
LO	*Raphidodiscus marylandicus*		16.7	
LO	*Thalassiosira bukryi*	(B subzone–*D. nicobarica*)	17.0	x
FO	*Coscinodiscus blysmos*		17.1	
FO	*Craspedodiscus coscinodiscus* s. str.		17.3	
FO	*Annellus californicus*		17.3	
FO	*Coscinodiscus lewisianus* var. *similis*		17.4	
FO	*Denticulopsis nicobarica*	(*D. nicobarica*)	17.8	x
LO	*Thalassiosira spinosa*		17.9	
LO	*Actinocyclus radionovae*		18.0	x
LO	*Craspedodiscus elegans*	(*T. pileus*)	18.7	
FO	*Nitzschia maleinterpretaria*		18.8	
FO	*Thalassiosira fraga*		19.9	
LO	*Bogorovia veniamini*	(*C. elegans*)	19.9	x
LO	*Coscinodiscus oligocenicus*	(C subzone–(*R. paleacea*)	20.6	
LO	*Melosira architecturalis*		20.9	
FO	*Actinocyclus radionovae*		21.2	
LO	*Thalassiosira primalabiata*	(B subzone–(*R. paleacea*)	21.7	
FO	*Craspedodiscus elegans*		22.2	
LO	*Coscinodiscus lewsianus* var. *rhomboides*		22.5	
FO	*Rossiella paleacea*	(*R. paleacea*)	22.7	
LO	*Rocella gelida*		22.7	
FO	*Rocella gelida* var. *schraderi*		23.6	
Oligocene/Miocene boundary			23.7	
FO	*Rocella gelida*	(*R. gelida*)	24.0	
FO	*Bogorovia veniamini*	(*B. veniamini*)	26.5	
LO	*Cestodiscus mukhinae*	(B subzone–*R. vigilans*)	28.5	
LO	*Coscinodiscus excavatus*	(*R. vigilans*)	34.0	
Eocene/Oligocene boundary			36.2	
FO	*Coscinodiscus excavatus*	(*C. excavatus*)	36.5	

Note: FO = first occurrence and LO = last occurrence. All zonal assignments refer to the bottom boundary of the zone or subzone. The age estimates are derived from Barron (1985a, 1985b) and Barron et al. (1985a). Species events which have a direct tie to a paleomagnetic time scale are marked with an "x" in the magnetic calibration (MAG) column.

netic polarity time scale of Berggren et al. (1985a, 1985b) (Table 7). We employed a slight modification of the nomenclature adopted by those authors. For the upper part of the time scale (roughly Pliocene-Pleistocene), we used the traditional proper or place names to refer to various chrons or subchrons. Below this, we followed the convention of using correlative anomaly numbers prefaced by the letter C. Normal polarity subchrons are referred to by adding suffixes (e.g., N1, N2), which increase with age.

Magnetic Experiments

Magnetic experiments conducted in the shipboard paleomagnetics laboratory can be grouped under three headings: (a) pass-through magnetometer measurements, (b) discrete sample paleomagnetic measurements, and (c) low-field susceptibility measurements. Objectives and procedures for each of the three types of magnetic analyses are described below.

Pass-Through Magnetometer

Pass-through magnetometer measurements were made using a superconducting cryogenic magnetometer. These measurements were performed on archive split-core sections at intervals of 5–10 cm, which corresponds roughly to the spatial resolution of the instrument. Natural remanent magnetization (NRM) measurements and/or measurements after blanket demagnetization treatments of 5–9 mT give a relatively complete record of magnetization directions through the core. This sequence of directions provides the basis for the initial interpretation of magnetic polarity stratigraphy.

Discrete Sampling

Discrete sample measurements were made using either the superconducting cryogenic magnetometer or the Minispin fluxgate magnetometer. These measurements allow a more thorough analysis of the character of the magnetization since individual samples can be subjected to full, progressive alternating-field (AF) demagnetization up to 100 mT. Such detailed analysis is necessary both for establishing appropriate blanket treatments and for accurately determining paleomagnetic inclination values.

Low-Field Susceptibility

Whole-core volume magnetic susceptibility measurements were made using a Bartington Susceptibility Meter (Model MS1) and a whole-core, pass-through sensor coil of 80-mm inner diameter (Model MS2C). Measurements were made at varying intervals

Table 7. Geomagnetic polarity time scale for the Cenozoic (after Berggren et al., 1985a, 1985b).

Normal polarity interval (Ma)	Anomaly
0–0.73	1
0.91–0.98	
1.66–1.88	2
2.02–2.04	
2.12–2.14	
2.47–2.92	2A
2.99–3.08	2A
3.18–3.40	2A
3.88–3.97	3
4.10–4.24	3
4.40–4.47	3
4.57–4.77	3
5.35–5.53	3A
5.68–5.89	3A
6.37–6.50	
6.70–6.78	4
6.85–7.28	4
7.35–7.41	4
7.90–8.21	4A
8.41–8.50	4A
8.71–8.80	
8.92–10.42	5
10.54–10.59	
11.03–11.09	
11.55–11.73	5A
11.86–12.12	5A
12.46–12.49	
12.58–12.62	
12.83–13.01	
13.20–13.46	
13.69–14.08	
14.20–14.66	
14.87–14.96	5B
15.13–15.27	5B
16.22–16.52	5C
16.56–16.73	5C
16.80–16.98	5C
17.57–17.90	5D
18.12–18.14	5D
18.56–19.09	5E
19.35–20.45	6
20.88–21.16	6A
21.38–21.71	6A
21.90–22.06	
22.25–22.35	
22.57–22.97	6B
23.27–23.44	6C
23.55–23.79	6C
24.04–24.21	6C
25.50–25.60	7
25.67–25.97	7
26.38–26.56	7A
26.86–26.93	8
27.01–27.74	8
28.15–28.74	9
28.80–29.21	9
29.73–30.03	10
30.09–30.33	10
31.23–31.58	11
31.64–32.06	11
32.46–32.90	12
35.29–35.47	13
35.54–35.87	13
37.24–37.46	15
37.48–37.68	15
38.10–38.34	16
38.50–38.79	16
38.83–39.24	16
39.53–40.43	17
40.50–40.70	17

Table 7 (Continued).

Normal polarity interval (Ma)	Anomaly
40.77–41.11	17
41.29–41.73	18
41.80–42.23	18
42.30–42.73	18
43.60–44.06	19
44.66–46.17	20
48.75–50.34	21
51.95–52.62	22
53.88–54.03	23
54.09–54.70	23
55.14–55.37	24
55.66–56.14	24
58.64–59.24	25
60.21–60.75	26
63.03–63.54	27
64.29–65.12	28
65.50–66.17	29
66.74–68.42	30

(3, 5, 6, 7, or 10 cm), depending on the rate of recovery, homogeneity of the sediment, and degree of disturbance of the core material.

Whole-core susceptibility measurements provide an indication of the amount of magnetizable material in the sediment. Magnetizable sedimentary constituents include not only "ferromagnetic" (NRM-carrying) minerals like magnetite, maghemite, hematite, goethite, and pyrrhotite, etc., but also paramagnetic minerals such as clays, ferromagnesian silicates, and colloidal iron/manganese-oxyhydroxide complexes (i.e., "limonite") in pore waters.

Biogenic carbonates and silica, in contrast, are diamagnetic (i.e., they exhibit negative susceptibility values). Downhole fluctuations in whole-core susceptibility, therefore, often reflect variations in the lithology of cored sequences; that is, changes in the ratio of biogenic (diamagnetic) to lithogenic (paramagnetic and ferromagnetic) components in the sediment. Accordingly, simple, rapid, and nondestructive whole-core measurements of volume magnetic susceptibility provide a means of regional-scale lithostratigraphic correlation between holes.

Whole-core susceptibility measurements are also useful in identifying intervals in cored sequences that have been contaminated by rust particles from the drill pipe or bit (Sager, 1986).

GEOCHEMISTRY

Interstitial Waters

We routinely collected interstitial water samples and analyzed them on board ship for pH, alkalinity, salinity, calcium, magnesium, sulfate, and chlorinity. In addition, we also determined phosphate, ammonia, and silica amounts for Leg 115. Water was squeezed from the sediments using a stainless-steel press, collected in plastic syringes, and filtered through 0.22-μm, 1-in. millipore filters.

The pH was measured with a Metrohm 605 pH meter calibrated using a free hydrogen ion scale (Hansson, 1973). Buffers were made using TRIS-TRISHCl in 0.7 NaCl. Samples were subsequently titrated with 0.1N HCl made up in a 0.7-m NaCl solution, the end-point being calculated using the Gran Factor method. Calibration was achieved by titrating 2 and 4 mmol $NaHCO_3$ solutions made in a 0.7-m NaCl solution.

We determined salinity values from the refractive index as measured by an AO Scientific Instruments optical refractometer. Calcium concentrations were determined by complexometric titration of a 0.5-mL sample with EGTA, using GHA as an end-point indicator. In order to enhance the detection of this end-point, the calcium-GHA complex was extracted into a layer of butanol (Gieskes, 1973). No correction was made for strontium. The magnesium content was determined by EDTA titration for total alkaline earths (Gieskes, 1974) and subsequently corrected for calcium. Sulfate concentrations were measured using a Dionex 2120i Ion Chromatograph, calibrated using a range of synthetic standards approximating seawater composition. Chlorinity was determined by titration with silver nitrate, using potassium chromate as an end-point indicator.

We used a spectrophotometer to measure concentrations of ammonia, phosphate, and silica. For ammonia, 10 μL of the sample was treated in an alkaline citrate medium with sodium hypochlorite and phenol in the presence of sodium nitroprusside. Silica was determined by producing a silicomolybdate complex and subsequently reducing it to form a blue complex after the method of Mann and Gieskes (1975). The measurement of phosphate was adapted from Strickland and Parsons (1968) and Presley (1971).

Surface seawater was routinely collected at each site and analyzed using identical chemical procedures. For purposes of comparison, data were plotted and listed at a depth of 0 m in the "Geochemistry" sections of each site chapter.

Carbonate and Organic Carbon Determinations

Inorganic carbon (carbonate) was determined using a Coulometrics Carbon Dioxide Coulometer. The sample was treated with HCl, and the evolved CO_2 was transferred to the CO_2 coulometer cell. This cell was filled with a partially aqueous medium containing ethanolamine and a coulometric indicator. When CO_2 was passed through the solution, the CO_2 was quantitatively absorbed and converted to a strong titratable acid by the ethanolamine. The coulometer electrically generated base to return the indicator color to the starting point. Electronic scaling within the coulometer converted the number of coulombs to a digital readout of micrograms of carbon. The relative error of this technique is approximately 1%.

We calculated total organic carbon (TOC) by calculating the difference between the total carbon (from the PE 240C Analyzer) and the inorganic carbon (from the coulometer). As a result of taking standard measurements during Leg 115, the detection limit using this method was found to be relatively high (0.5%) in carbonate-rich sediments.

XRD Analyses

A Philips ADP 3520 X-ray diffractometer was used for X-ray diffraction (XRD) analysis. All sediment samples squeezed for interstitial water analysis, in addition to some physical properties samples, were analyzed by two methods:

1. In the first method, the percentages of calcite, aragonite, quartz, and dolomite were determined by comparison with a suite of standards. These standards enabled a calibration line to be calculated between mineral percentage and peak area (or height), and an estimate to be made of the percent error in the determinations.
2. In the second method, samples were subjected to a scan between 20° and 40° 2 theta (θ) to identify other minerals present.

Instrument conditions were as follows:

CuK_α radiation with Ni filter
40 kV
35 mA
Continuous scan from 2° to 60° 2 θ

Resulting diffractograms were identified with the help of a computerized search-and-match routine using Joint Committee on Powder Diffraction Standards (JCPDS) powder files.

Gas Analysis

Analyses for head-space gases were conducted on all samples analyzed for their interstitial waters. The procedure consisted of sealing a small portion of a sample in a 20-cm^3 glass vial with a crimped metal cap. The vial was then heated at 70°C for 1 hr, and concentrations of C_1, C_2, C_3, and C_4 gases were measured by gas chromatography.

BASEMENT DESCRIPTION CONVENTIONS

Core Handling

Each core of igneous rock was divided into 1.5-m sections, and the pieces within these sections were examined to determine if the orientation of the piece had been preserved during coring and handling. If the orientation had been preserved, the bottom of the piece was marked. The pieces were then cut into *archive* and *working* halves using a rock saw with a diamond blade. The cut halves were laid in a split core liner, and pieces that fit together were separated from the next piece with a plastic separator that was glued into the core liner.

Each piece of rock was numbered sequentially from the top of each core section, beginning with the number 1. Pieces were labeled on the rounded, not the sawed, surface. Pieces that could be fit together (reassembled like a jigsaw puzzle) were given the same number, but were lettered consecutively downsection, as 1A, 1B, 1C, and so on. Some numbered and lettered pieces (e.g., 1A) broke after labeling, and the pieces were assigned additional subnumbers, as 1A1, 1A2, and so on. Whenever the orientation of the piece was preserved, an arrow was added to the label pointing to the top of the section. The *archive* halves of all cores were photographed.

Visual Core Descriptions

We divided each core into lithologic units based on texture, mineralogy, alteration, intercalated sediment, and glassy contacts. The units were numbered consecutively from the top of the core downward. Pieces from the *archive* half were drawn in the left-hand column of the ODP visual core description form for igneous/metamorphic rocks (Fig. 9), and the location of plastic separators was indicated by a solid line drawn across the column.

Each unit was described in terms of primary and secondary mineralogy, texture, color, vesicularity, voids, fractures, and alteration. This information was also entered on the visual core description forms. These forms and the photographs of the *archive* half are presented in the appropriate site chapters in this volume.

The texture of the basalts was described as aphyric if phenocrysts amounted to less than 1% of the rock, sparsely porphyritic if phenocryst content ranged from 1% to 2%, moderately porphyritic at 2% to 10%, and highly porphyritic if phenocrysts amounted to more than 10% of the rock.

Samples for shipboard and shore-based analyses were removed from the *working* half and were identified by hole, core, section, interval, and piece number. The type of measurement and approximate sample interval are indicated on the visual core description forms in the column headed "Shipboard Studies," using the following notation:

PM = paleomagnetic measurements
TS = thin-section billet
PP = physical properties measurements
TC = thermal conductivity
PH = photograph

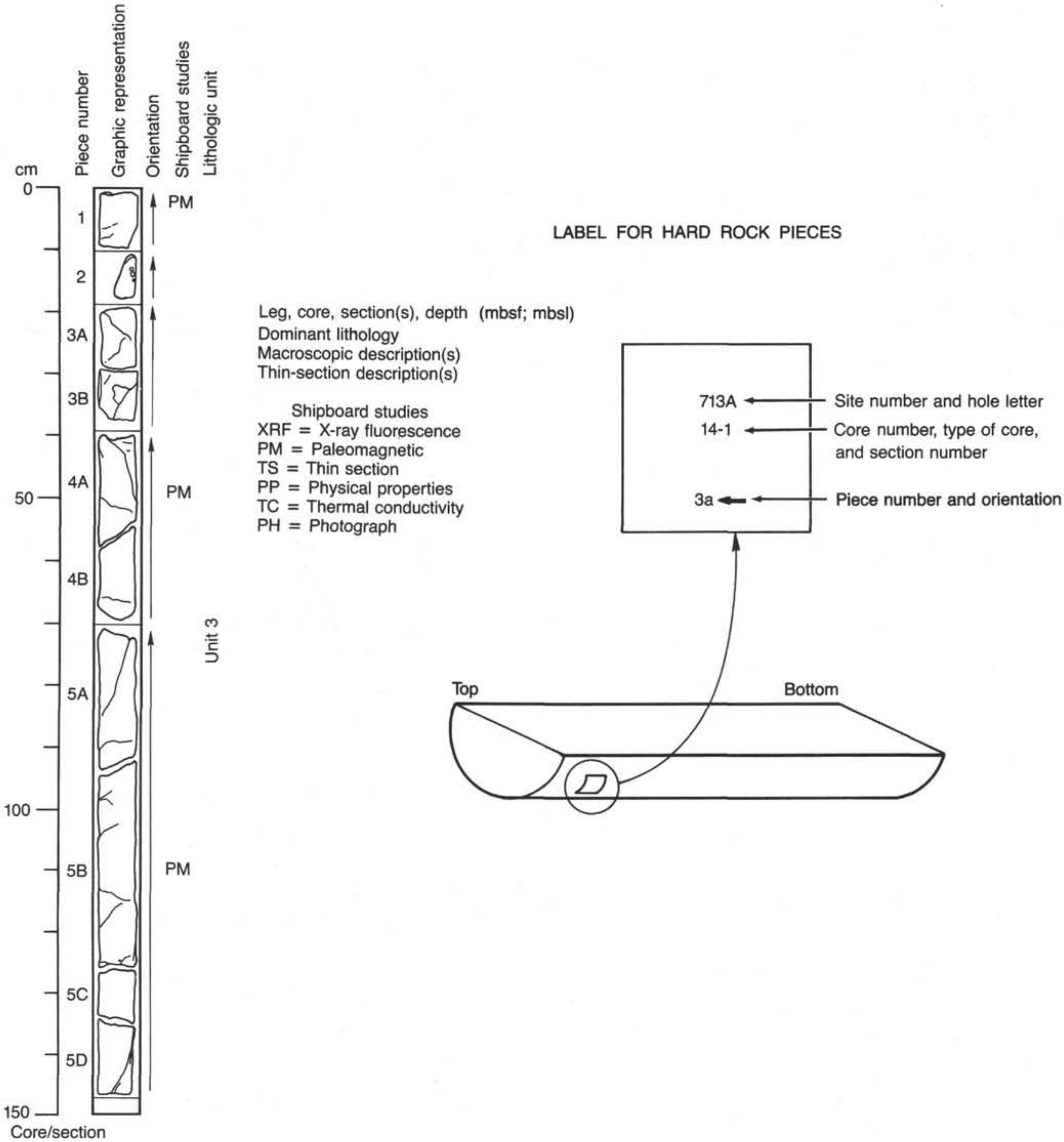

Figure 9. Core description forms used for igneous and metamorphic rocks, and diagram showing labeling of hard-rock pieces.

Shipboard measurements of physical properties and magnetic properties were routinely made upon minicores, some of which were then subdivided for X-ray fluorescence (XRF) analysis and manufacture of a thin section, in order to ensure that as many measurements as possible could be correlated directly. Thin sections made on board were described, and the descriptions were recorded on thin-section description forms.

Igneous Rock Classification

We used the I.U.G.S. classification scheme to classify igneous rocks, relying mainly on the descriptions of mineralogy and texture. Basalts were called aphyric if phenocrysts amounted to less than 1% of the rock. Basalts were classified by phenocryst type (e.g., an olivine-plagioclase basalt). If more than one phenocryst phase was present, then both were used in increasing order of abundance.

Thin-Section Billets

Thin sections were made from most units of basaltic rock recovered during Leg 115. These were examined to refine unit boundaries indicated by hand-specimen core descriptions, to confirm the identity of the petrographic groups represented in the cores, and to define their secondary alteration mineralogy. Features of the thin sections that were noted included: the texture, mineral type, morphology, abundance, zoning, and twinning; the presence of xenocrysts; secondary mineral type and abundance; and the presence of vein, vesicle, and fracture filling. This information is reported on the detailed thin-section description forms.

Basement Alteration

Alteration effects due to seawater interaction with igneous rocks were described in hand specimens and thin sections. The color of any alteration halos around fractures or vugs was noted, and the total percentage of veins and fracture fillings and their thicknesses were estimated in the core descriptions. The identities of secondary minerals that filled fractures and vesicles or replaced igneous phases were estimated in visual core descriptions, and these estimates refined in thin section. The total percentages of the various secondary minerals were also estimated from thin-section examinations.

XRF Analyses

Samples considered by the shipboard party to be representative of individual lithologic units, or possibly of unusual composition, were analyzed for major and trace elements by XRF. The on-board XRF system (Applied Research Laboratory 8420) is a fully automated, wavelength-dispersive, X-ray fluorescence spectrometer using a 3-kW rhodium X-ray tube as the excitation source for both major and trace elements. The elements analyzed were silica, titanium, aluminum, iron, manganese, magnesium, calcium, sodium, potassium, phosphorus, niobium, zirconium, yttrium, strontium, rubidium, zinc, copper, nickel, chromium, vanadium, cesium, and barium.

Much of the work in the XRF lab on board *JOIDES Resolution* has been aimed at developing sample preparation techniques and data reduction routines that are flexible and streamlined yet provide high-quality chemical data to the shipboard scientists. The scientists and technicians who sailed on Legs 109 and 111 had great success toward achieving this goal, and we used these techniques with few changes on Leg 115. The most important change we made was in using calculated backgrounds for silica, sodium, and magnesium calibration instead of using only measured backgrounds for major elements calibration.

We performed XRF analyses on 81 samples, and these analyses are listed in their respective sections.

PHYSICAL PROPERTIES

Introduction

The physical properties of sediments and rocks obtained from ocean drilling provide an important link between geophysical and geological data. Seismic and downhole logging records can be related through the physical properties to the geological description of cores given by shipboard stratigraphers, sedimentologists, and petrologists. The combination of these three data sets provides a comprehensive view of the seafloor geologic setting around the borehole.

The objectives of the physical properties program for Leg 115, in addition to aiding the geophysical interpretation, were the following: (1) to establish the influence of changes in carbonate content upon the generation of seismic reflectors; (2) to obtain high-resolution velocity and density profiles in order to construct synthetic seismograms; and (3) to create a data base for the formulation of a geoacoustic model characterizing carbonate-rich sediments. Note that pressure and temperature corrections have to be applied to laboratory velocity and density measurements for *in-situ* conditions. This is important for synthetic seismograms generated for lithostratigraphic studies.

The following measurements were determined from whole-core logs on 1.5-m long sections or from discrete samples:

1. Index properties: gravimetric and volumetric determination of wet-bulk density, dry-bulk density, grain density, porosity, and water content.
2. Carbonate analysis.
3. Gamma ray attenuation and porosity evaluation (GRAPE): continuous wet-bulk density determination.
4. Compressional-wave velocity: speed of sound obtained continuously using the *P*-wave logger or on discrete samples using a velocimeter.
5. Shear-wave velocity.
6. Vane shear strength: a measure of the maximum resistance of the sample to a torsional stress.
7. Thermal conductivity: a measure of the ability of the sample to transmit heat.

Note that measurements 3 and 5 were not possible for nonsedimentary materials. Wherever possible, discrete measurements were made contiguously within the same interval of core.

Index Properties

The measurement of wet and dry weights and volumes of selected samples allowed us to calculate various related index properties. Wet- and dry-bulk densities were determined in addition to other gravimetric parameters (defined below) using samples of approximately 20 cm^3. Wet and dry weights were determined on board using a Scitech electronic balance to an accuracy of ± 0.01 g. Sample volumes were calculated for both the wet and dry samples with a Penta Pyncnometer. Samples were dried by a freeze drier.

The following index properties were calculated using the volume-of-solids method described by Hamilton (1971), with a salinity correction of 35 ‰:

1. Wet-water content (%) $= \dfrac{\text{weight of seawater}}{\text{weight of wet sediment}} \times 100.$

2. Porosity (%) $= \dfrac{\text{volume of pore space}}{\text{volume of wet sediment}} \times 100.$

3. Wet-bulk density (g/cm^3) $= \dfrac{\text{weight of wet sediment}}{\text{volume of wet sediment}}.$

4. Dry-bulk density (g/cm^3) $= \dfrac{\text{weight of dry sediment}}{\text{volume of wet sediment}}.$

5. Grain density (g/cm^3) $= \dfrac{\text{weight of dry sediment}}{\text{volume of dry sediment}}.$

Carbonate Analysis

The carbonate content was calculated using coulometric techniques described in the "Geochemistry" section of this chapter. We determined carbonate contents on the samples used for index properties to an accuracy of 1 wt%.

GRAPE

The gamma ray attenuation porosity evaluator (GRAPE) consists of a gamma-ray source which radiates gamma rays through a whole-round section of core (which passes the source on a track) and a detector. The ratio of transmitted to detected intensity is dependent on the wet-bulk density of the material in the section. Further details on the use of the device are described by Boyce (1976).

The GRAPE system was calibrated periodically with an aluminum standard using the methods described in Boyce (1976), and an accuracy of 5% was achieved under normal operating conditions. The density of selected hard-rock samples was determined to within ±2% by using a 2-min exposure to the gamma ray with methods described by Boyce (1976). The GRAPE density values were strongly affected by the degree to which the core material filled the liner and by the presence of breaks in the sediment within the sections.

Compressional-Wave Velocity

Two different techniques were used to evaluate compressional velocities (V_p): (1) a whole-round core logging device—the *P*-wave logger (Schultheiss, Meinert, et al., 1988)—that allowed V_p to be determined at 1-mm intervals along the length of each core (in a direction perpendicular to the major core axis), and (2) a Hamilton Frame Velocimeter (Boyce, 1973) that allowed V_p to be obtained on selected discrete samples (in a direction parallel to the major core axis). All velocities were measured at atmospheric pressure and the *P*-wave logger results were corrected to a temperature of 20°C. Hamilton Frame measurements were not corrected for temperature variations as the cores had equilibrated to room temperature (24.5°C). Average core temperature was 22°C.

The *P*-wave logger was mounted beside the GRAPE, and a 1-MHz pulse was transmitted through cores as they passed by on a track. The traveltime of the pulse was measured by an automatic detection unit, as was the separation of the 1-MHz transducers, and V_p was calculated from these two measurements (Schultheiss, Meinert, et al., 1988). An accuracy of 1% was obtained under ideal operating conditions; however, the accuracy deteriorated to 2% for many practical applications because of electronic and mechanical noise.

We evaluated V_p using the Hamilton Frame Velocimeter (at 400 kHz) following the procedure described by Boyce (1973), with the addition of an automatic timing circuit to give a consistent method for determining traveltimes. An accuracy of ±2% was achieved; however, many brittle samples fractured on insertion into the device, increasing the uncertainty.

Shear-Wave Velocity

Ultrasonic shear-wave velocities (V_s) were measured at various locations within split sections of core. Piezoelectric bender transducers were inserted into unlithified sediments and a pulse detection circuit, similar to that used for the Hamilton Frame Velocimeter, was used to evaluate the traveltime between the transducers. The transducer separation was measured using vernier calipers allowing V_s to be calculated. Calculated V_s measurements were assigned an error of 20% (a maximum value), due to inaccuracies in the determination of the traveltime introduced by uncertainties in interpretation of the detected pulse. Further details of the technique are given by Schultheiss (1985).

Shear Strength

The shear strengths of various unlithified sediments were measured next to V_s locations in the freshly split sections, using a motorized shear vane device. A vane was inserted into the freshly split sections and a torsional stress applied to it. The maximum torque required to cause sediment failure was measured by a calibrated spring. The shear strength was calculated using the stress at failure and a geometric-size constant for the vane. The rotation rate was 60°/min. There is no easy way to assess the errors involved in obtaining the shear strength as it is a device-dependent measurement. Further details of experimental techniques are given by Boyce (1977).

Thermal Conductivity

The thermal conductivity of selected sections was measured using the needle-probe technique after the method of Von Herzen and Maxwell (1959). The needle probe consisted of a fine needle 1 mm in diameter which was inserted into whole-round sections through small holes drilled in the core liner. Measurements on lithified sediments and basalts were made using the half-space technique (Von Herzen and Maxwell, 1959), where a flat-faced sample was abutted against the face of a fused silica plate containing a needle probe. The measurement period was 6 min, recorded after a delay of a few hours to allow the sections to equilibrate to room temperature. Ambient temporal drift was measured by inserting an additional probe into a rubber standard. A drift of less than 4×10^{-2}°C/min was essential for reliable data.

Accumulation Rates

Accumulation rates, necessary for balancing the sedimentary flux, were calculated using the following equations:

Bulk accumulation rate (g/cm^2/1000 years) = sedimentation rate (cm/1000 years) × dry-bulk density (g/cm^3).

Carbonate accumulation rate (g/cm^2/1000 years) = bulk accumulation rate (g/cm^2/1000 years) × fractional carbonate content.

Noncarbonate accumulation rate (g/cm^2/1000 years) = bulk accumulation rate − carbonate accumulation rate.

DOWNHOLE LOGGING

The purpose of downhole logging is the direct determination of properties of *in-situ* formations adjacent to the borehole wall. After coring is completed at a hole, a tool string is lowered downhole on a coaxial cable, with each of several tools in the tool string continuously monitoring some property of the adjacent borehole. Of the dozens of different tool strings in common use in the petroleum industry, three were selected for use on Leg 115: the Schlumberger seismic stratigraphy combination (BHC, GR, DIL, and MCD), the Schlumberger geochemical combination (NGT, GST, and ACT), and the Schlumberger lithoporosity combination (NGT, LDT, and CNTG).

Log Types

The physical principles and properties of the Schlumberger tools are described in previous shipboard reports and many publications (e.g., Schlumberger, 1972; Serra, 1984; Borehole Research Group, 1985) and are not repeated here in any detail.

The seismic stratigraphic combination consists of the borehole compensated sonic tool (BHC), gamma-ray tool (GR), dual induction resistivity tool (DIL), and caliper tool (MCD). The geochemical combination includes the natural gamma spectrometry tool (NGT), induced gamma-ray spectrometry tool (GST), and the aluminum clay tool (ACT). The lithoporosity combination includes the natural gamma spectrometry tool (NGT), lithodensity tool (LDT), and the compensated neutron tool (CNTG). We included an additional tool on the lithoporosity combination, the three-axis magnetometer tool (GPIT).

The BHC tool has two transducers and two receivers, permitting measurements of sonic traveltime over distances of 2.4, 3.0, and 3.7 m. Two logs are recorded: the shorter-spaced dead-reckoning (DR) log measures the traveltime difference for the 0.6-m interval between the 2.4- and 3.0-m transducer/receiver pairs. Traveltimes are based on a simple first-break threshold criterion. Waveforms were recorded during logging upward but could not be analyzed until after the cruise.

The DIL tool records three resistivity logs with different depths of penetration: the spherically focused log (SFL) penetrates less than 50 cm into the formation, the medium induction laterolog (ILM) penetrates about 1–2 m, and the deep induction laterolog (ILD) penetrates about 2 m. The resistivity logs respond primarily to formation porosity (assuming absence of hydrocarbons). Some lithologic response also occurs associated with bound water in clays.

The caliper (MCD) is a three-arm (bowspring) device which measures hole diameter. It is used primarily for quality control and environmental correction of other types of logs.

The gamma-ray (GR) tool measures the natural gamma-ray emissions of the formation. Radioactive decay of potassium, uranium, and thorium contributes to the measured signal, but the potassium contribution is usually dominant. Traditionally considered a sand/shale indicator, the tool is more correctly described as an indicator of the relative proportion of quartz and carbonate to clay minerals because it responds to mineralogy rather than grain size. Potassium feldspars can dominate the gamma-ray response but are usually minor in comparison to potassium-bearing clays.

The neutron tool (CNTG) uses a radioactive source to bombard the formation with neutrons. Neutrons with both "thermal" and "epithermal" energy states are captured by nuclei in the formation. Each capture is accompanied by gamma-ray emission with an energy state dependent on the type of atom; the CNTG measures the amount of capture resulting from hydrogen. In hydrocarbon-free formations, the CNTG therefore measures total water content of the formation, including both pore spaces and bound water in clay minerals.

The natural-gamma-ray tool (NGT) is somewhat similar to the standard gamma-ray tool (GR) in that both measure natural gamma radiation emitted by formation rocks during radioactive decay of potassium, uranium, and thorium. Unlike the GR tool, which only measures total gamma rays, the NGT analyzes the spectral distribution of the gamma rays to provide accurate concentrations for the three elements. Potassium and thorium concentrations and their ratio are useful in determining the types of clay minerals present. Uranium commonly accumulates along faults or fractures; thus, uranium concentration can be a fracture indicator.

The ACT tool is an NGT tool which has been modified to be run below a CNTG tool with a californium radioisotope source of 2 Mev neutrons. It measures aluminum and manganese concentrations.

The lithodensity tool (LDT) provides a measure of formation bulk density and porosity. A radioactive source mounted on a pad applied to the hole wall by an eccentering arm emits gamma rays into the formation. The gamma rays are scattered through collisions with atoms of the formation, losing energy until they are absorbed through the photoelectric effect. The number of scattered gamma rays reaching two detectors (short and long) at fixed distances from the source is related to the electron density of the formation, which in turn depends on the true bulk density.

The gamma-ray spectrometry tool (GST) irradiates the formation with high-intensity (14 MeV) neutrons and measures the spectra of the resulting induced gamma rays. The tool measures the proportions of calcium, chlorine, silicon, iron, hydrogen, and sulfur. These abundances (except for iron) can be measured through the drill pipe.

The three-axis magnetometer tool (GPIT) is a general purpose instrumentation tool which measures 3-component accelerations and 3-component magnetic field strengths. It was used on this leg to study the magnetic field of the drilling assembly near the end of the drill pipe.

All log measurements are subject to error. All can be affected to some extent by hole conditions, such as changes in hole diameter, extensively caved intervals (washouts), fracturing, or alteration. The optimum logs to use in any hole may depend, therefore, on anticipated or experienced hole conditions as well as on scientific goals. Increasing the number of logs run causes a corresponding increase in the degree to which minor lithologic variations can be determined. Even a full suite of logs cannot compete with detailed core analysis of a single sample. Thus, the primary value of logs for lithology, porosity, and chemical determination lies in the fact that these variables are measured quickly and continuously over the entire logged interval. These determinations are, of course, most valuable in intervals of poor or disturbed core recovery. Porosity determination through logs has the additional virtue of measuring *in-situ* porosity prior to core disturbance by drilling or core expansion from pressure release.

Log Analysis

During logging, incoming data were observed in real time on a monitor oscilloscope and simultaneously recorded on digital tape in the Schlumberger logging unit. After logging, this tape was copied from 800 to 1600 bpi on the shipboard Vax computer system. The 1600-bpi tape was then read by the Masscomp computer system in Downhole Logging aboard ship, and reformatted to a file format compatible with the Terralog log interpretation software package. Rather than a "black box," Terralog is an interactive system consisting of a large number of log manipulation and plot options. Thus, the log analysis and interpretation varied in duration and procedure for each site. Preliminary log interpretation was carried out on board; more detailed analyses are under way and will be presented in the *Scientific Results* portion of the Leg 115 *Proceedings* volume.

OBTAINING SAMPLES

Potential investigators wanting to obtain samples should refer to the ODP-NSF Sample Distribution Policy. Sample-request forms may be obtained from the Curator, Ocean Drilling Program, 1000 Discovery Drive, College Station, Texas 77840. Requests must be as specific as possible: include site, hole, core, section, interval within a section, and volume of sample required.

REFERENCES

Backman, J., 1986. Quantitative calcareous nannofossil biochronology of middle Eocene through early Oligocene sediment from DSDP Site 522 and 523. *Abh. Geol. Bundesanst. Austria*, 39:21–31.

Backman, J., and Pestiaux, P., 1986. Pliocene *Discoaster* abundance variations, Deep Sea Drilling Project Site 606: biochronology and paleoenvironmental implications. *In* Ruddiman, W. F., Kidd, R. B., Thomas, E., et al., *Init. Repts. DSDP*, 94, Pt. 2: Washington (U.S. Govt. Printing Office), 903–910.

Backman, J., and Shackleton, N. J., 1983. Quantitative biochronology of Pliocene and early Pleistocene calcareous nannofossils from the Atlantic, Indian and Pacific oceans. *Mar. Micropaleontol.*, 8:141–170.

Baldauf, J. G., 1985a. A high resolution late Miocene–Pliocene diatom biostratigraphy for the eastern equatorial Pacific. *In* Mayer, L., Theyer, F., et al., *Init. Repts. DSDP*, 85: Washington (U.S. Govt. Printing Office), 457–475.

________, 1985b. Cenozoic diatom biostratigraphy and paleoceanography of the Rockall Plateau Region, North Atlantic, Deep Sea Drilling Project Leg 81. *In* Roberts, D., Schnitker, D., et al., *Init. Repts. DSDP*, 81: Washington (U.S. Govt. Printing Office), 439–478.

Baldauf, J. G., Thomas, E., Clement, B., Takayama, T., Weaver, P.P.E., Backman, J., Jenkins, G., Mudie, P. J., and Westberg-Smith, M. J., 1987. Magnetostratigraphic and biostratigraphic synthesis, Deep Sea Drilling Project Leg 94. In Ruddiman, W. F., Kidd, R. B., Thomas, E., et al., *Init. Repts. DSDP*, 94, Pt. 2: Washington (U.S. Govt. Printing Office), 1159–1205.

Barron, J. A., 1980. Upper Pliocene and Quaternary diatom biostratigraphy of Deep Sea Drilling Project Leg 54, tropical eastern Pacific. *In* Rosendahl, B. R., Hekinian, R., et al., *Init. Repts. DSDP*, 54: Washington (U.S. Govt. Printing Office), 455–485.

———, 1983. Latest Oligocene through early middle Miocene diatom biostratigraphy of the eastern tropical Pacific. *Mar. Micropaleontol.*, 7:487–515.

———, 1985a. Late Eocene to Holocene diatom biostratigraphy of the equatorial Pacific Ocean, Deep Sea Drilling Project Leg 85. *In* Mayer, L., Theyer, F., et al., *Init. Repts. DSDP*, 85: Washington (U.S. Govt. Printing Office), 413–456.

———, 1985b. Miocene to Quaternary planktic diatom biostratigraphy. *In* Bolli, H. M., Saunders, J. B., and Perch-Nielsen, K. (Eds.), *Plankton Stratigraphy:* Cambridge (Cambridge Univ. Press), 763–809.

Barron, J. A., Keller, G., and Dunn, D. A., 1985a. A multiple microfossil biochronology for the Miocene. *In* Kennett, J. P. (Ed.), *The Miocene Ocean: Paleoceanography and Biogeography*. Geol. Soc. Am. Mem., 163:21–36.

Barron, J. A., Nigrini, C. A., Pujos, A., Saito, T., Theyer, F., Thomas, E., and Weinreich, N., 1985b. Synthesis of biostratigraphy, central equatorial Pacific, Deep Sea Drilling Project Leg 85: refinement of Oligocene to Quaternary biochronology. *In* Mayer, L., Theyer, F., et al., *Init. Repts. DSDP*, 85: Washington (U.S. Govt. Printing Office), 905–934.

Barton, C. E., and Bloemendal, J., 1986. Paleomagnetism of sediments collected during Leg 90, southwest Pacific. *In* Kennett, J. P., von der Borch, C. C., et al., *Init. Repts. DSDP*, 90: Washington (U.S. Govt. Printing Office), 1273–1316.

Berggren, W. A., Kent, D. V., and Flynn, J. J., 1985a. Jurassic to Paleogene: Part 2. Paleogene geochronology and chronostratigraphy. *In* Snelling, N. J. (Ed.), *The Chronology of the Geological Record*, Geol. Soc. London Mem., 10:141–195.

Berggren, W. A., Kent, D. V., and Van Couvering, J. A., 1985b. The Neogene: Part 2. Neogene geochronology and chronostratigraphy. *In* Snelling, N. J. (Ed.), *The Chronology of the Geological Record*, Geol. Soc. London Mem. 10:211–260.

Blow, W. H., 1969. Late middle Eocene to Recent planktonic foraminiferal biostratigraphy. *Proc. 1st Intl. Conf. Planktonic Microfossils*, 1: 199–422.

Boersma, A., and Premoli Silva, I., 1986. Terminal Eocene event: Planktonic Foraminifera and isotopic evidence. *In* Pomerol, C., and Premoli Silva, I. (Eds.), *Terminal Eocene Events*: New York (Elsevier), 213–224.

Borehole Research Group, 1985. *Wireline Logging Manual*: Palisades, NY (Eldigio Press).

Boyce, R. E., 1973. Appendix I. Physical properties—methods. *In* Edgar, N. T., Saunders, J. B., et al., *Init. Repts. DSDP*, 15: Washington (U.S. Govt. Printing Office), 1115–1128.

———, 1976. Appendix I. Definitions and laboratory techniques of compressional sound velocity parameters and wet-water content, wet-bulk density, and porosity parameters by gravimetric and gamma-ray attenuation techniques. *In* Schlanger, S. O., Jackson, E. D., et al., *Init. Repts. DSDP*, 33: Washington (U.S. Govt. Printing Office), 931–958.

———, 1977. Deep Sea Drilling Project procedures for shear strength measurement of clayey sediment using modified Wykeham Farrance laboratory vane apparatus. *In* Barker, P. F., Dalziel, I.W.D., et al., *Init. Repts. DSDP*, 36: Washington (U.S. Govt. Printing Office), 1059–1068.

Bukry, D., 1973. Low-latitude coccolith biostratigraphic zonation. *In* Edgar, N. T., Saunders, J. B., et al., *Init. Repts. DSDP*, 15: Washington (U.S. Govt. Printing Office), 685–703.

———, 1975. Coccolith and silicoflagellate stratigraphy, northwestern Pacific Ocean, Deep Sea Drilling Project Leg 32. *In* Larsen, R. L., Moberly, R., et al., *Init. Repts. DSDP*, 32: Washington (U.S. Govt. Printing Office), 677–701.

Bukry, D., and Foster, J. H., 1973. Silicoflagellate and diatom stratigraphy, Leg 16, Deep Sea Drilling Project. *In* van Andel, T. H., Heath, G. R., et al., *Init. Repts. DSDP*, 16: Washington (U.S. Govt. Printing Office), 815–871.

Burckle, L. H., 1972. Late Cenozoic planktonic diatom zones from the eastern equatorial Pacific. *Nova Hedwigia, Beift.*, 39:217–205.

———, 1977. Pliocene and Pleistocene diatom datum levels from the equatorial Pacific. *Quat. Geol.*, 7:330–340.

———, 1978. Early Miocene to Pliocene diatom datum levels for the equatorial Pacific. *Bull. Geol. Res. Dev. Cent. Bandung, Indones.*, 1:25–44.

Burckle, L. H., and Opdyke, N. D., 1977. Late Neogene diatom correlations in the circum-Pacific. *Proc. 1st Intl. Congr. Pac. Neogene Stratigr.*: Tokyo (Kaiyo Shuppan), 255–284.

Burckle, L. H., and Trainer, J., 1979. Middle and late Pliocene diatom datum levels from the central Pacific. *Micropaleontology*, 25:281–293.

Burckle, L. H., Hammond, S. R., and Seyb, S. M., 1978. A stratigraphically important new diatom from the Pleistocene of the North Pacific. *Pac. Sci.*, 32:209–214.

Burckle, L. H., Keigwin, L. D., and Opdyke, N. D., 1982. Middle and late Miocene stable isotope stratigraphy: correlation to the paleomagnetic reversal record. *Micropaleontology*, 28:329–334.

Ciesielski, P. F., 1983. The Neogene and Quaternary diatom biostratigraphy of subantarctic sediments, Deep Sea Drilling Project Leg 71. *In* Ludwig, W. J., Krasheninnikov, V. A., et al., *Init. Repts. DSDP*, 71: Washington (U.S. Govt. Printing Office), 635–665.

Clement, B. M., and Robinson, F., 1987. The magnetostratigraphy of Leg 94 sediments. *In* Ruddiman, W. F., Kidd, R. B., et al., *Init. Repts. DSDP*, 94, Pt. 2: Washington (U.S. Govt. Printing Office), 635–650.

Dean, W. E., Leinen, M., and Stow, D.A.V., 1985. Classification of deep-sea, fine-grained sediments. *J. Sediment. Petrol.*, 55:250–256.

Dunham, R. J., 1962. Classification of carbonate rocks according to depositional texture. *AAPG Mem.*, 1:108–121.

Embry, A. F., and Klovan, J. E., 1971. A late Devonian reef tract on northeastern Banks Island, Northwest Territories. *Bull. Can. Pet. Geol.*, 19:730–781.

Fenner, J., 1985. Late Cretaceous to Oligocene planktic diatoms. *In* Bolli, H. M., Saunders, J. B., and Perch-Nielsen, K. (Eds.), *Plankton Stratigraphy*: Cambridge (Cambridge Univ. Press), 713–762.

Fleischer, R. L., 1977. Oligocene planktonic foraminiferal assemblages from DSDP sites in the Indian Ocean. *In* Heirtzler, J. R., et al. (Eds.), *Indian Ocean Geology and Biostratigraphy*: Washington (American Geophysical Union), 459–467.

Gartner, S., Jr., 1977. Calcareous nannofossil biostratigraphy and revised zonation of the Pleistocene. *Mar. Micropaleontol.*, 2:1–25.

Gieskes, J. M., 1973. Interstitial water studies, Leg 15: alkalinity, pH, Mg, Ca, Si, PO_4, and NH_4. *In* Heezen, B. C., MacGregor, I. G., et al., *Init. Repts. DSDP*, 20: Washington (U.S. Govt. Printing Office), 813–829.

———, 1974. Interstitial water studies, Leg 25. *In* Simpson, E.S.W., Schlich, R., et al., *Init. Repts. DSDP*, 25: Washington (U.S. Govt. Printing Office), 361–394.

Hamilton, E. L., 1971. Prediction of *in-situ* acoustic and elastic properties of marine sediments. *Geophysics*, 36:266–284.

Hansson, I., 1973. A new set of pH scales and standard buffers for seawater. *Deep-Sea Res.*, 20:479–491.

Johnson, D. A., and Nigrini, C. A., 1985. Synchronous and time-transgressive Neogene radiolarian events in the tropical Indian and Pacific Oceans. *Mar. Micropaleontol.*, 9:489–523.

Jousé, A. P., and Kazarina, G. H., 1974. Pleistocene diatoms from Site 262, Leg 27, DSDP. *In* Veevers, J. J., Heirtzler, J. R., et al., *Init. Repts. DSDP*, 27: Washington (U.S. Govt. Printing Office), 925–946.

Kennett, J. P., and Srinivasan, M. S., 1983. *Neogene Planktonic Foraminifera*: Stroudsburg, PA (Hutchison Ross).

Lohman, W. H., 1986. Calcareous nannoplankton biostratigraphy of the southern Coral Sea, Tasman Sea, and southwestern Pacific Ocean. Deep Sea Drilling Project Leg 90: Neogene and Quaternary. *In* Kennett, J. P., von der Borch, C. C., et al., *Init. Repts. DSDP*, 90: Washington (U.S. Govt. Printing Office), 763–795.

Mann, R., and Gieskes, J. M., 1975. Interstitial water studies, Leg 28. *In* Hayes, D. E., Frakes, L. A., et al., *Init. Repts. DSDP*, 28: Washington (U.S. Govt. Printing Office), 805–814.

Martini, E., 1971. Standard Tertiary and Quaternary calcareous nannoplankton zonation. *In* Farinacci, A. (Ed.), *Proc. II Planktonic Conf. Roma, 1971*: Rome (Ed. Tecnoscienza), 739–777.

Matsuoka, H., and Okada, H., in press. Quantitative analysis of Quaternary nannoplanktons in the subtropical northwestern Pacific Ocean. *Mar. Micropaleontol.*

Matthews, D. J., 1939. *Tables of Velocity of Sound in Pore Water and in Seawater*: London (Admiralty, Hydrogr. Dept.).

McFadden, P. L., and Reid, A. B., 1982. Analysis of paleomagnetic inclination data. *Geophys. J. R. Astron. Soc.*, 69:307–319.

McGowran, B., 1977. Maastrichtian to Eocene foraminiferal assemblages in the northern and eastern Indian Ocean region: correlations and historical patterns. *In* Heirtzler, J. R., et al. (Eds.), *Indian Ocean Geology and Biostratigraphy*: Washington (American Geophysical Union), 417–458.

Munsell Soil Color Charts, 1971. Baltimore (Munsell Color).

Nigrini, C. A., 1985. Radiolarian biostratigraphy in the central equatorial Pacific, Deep Sea Drilling Project Leg 85. *In* Mayer, L., Theyer, F., et al., *Init. Repts. DSDP*, 85: Washington (U.S. Govt. Printing Office), 511–551.

Nocchi, M., Parisi, G., Monaco, P., Monechi, S., Madile, M., Napoleone, G., Ripepe, M., Orlando, M., Premoli Silva, I., and Rice, D. M., 1986. The Eocene-Oligocene boundary in the Umbrian pelagic sequences, Italy. *In* Pomerol, C., and Premoli Silva, I. (Eds.), *Terminal Eocene Events*: New York (Elsevier), 25–40.

Okada, H., and Bukry, D., 1980. Supplementary modification and introduction of code numbers to the low-latitude coccolith biostratigraphic zonation (Bukry, 1973; 1975). *Mar. Micropaleontol.*, 5:321–325.

Poore, R. A., Tauxe, L., Percival, S. F., Jr., LaBrecque, J. L., Wright, R., Peterson, N. P., Smith, C. C., Tucker, P., and Hsü, K. J., 1983. Late Cretaceous-Cenozoic magnetostratigraphic and biostratigraphic correlations for the South Atlantic Ocean, DSDP Leg 73. *Palaeogeogr. Palaeoclimatol. Palaeoecol.*, 42:127–148.

Presley, B. J., 1971. Appendix: Techniques for analyzing interstitial water samples. Part I: Determination of selected minor and major inorganic constituents. *In* Winterer, E. L., Riedel, W. R., et al. *Init. Repts. DSDP*, 7: Washington (U.S. Govt. Printing Office), 1749–1755.

Pujos, A., 1985a. Quaternary nannofossils from Goban Spur, eastern North Atlantic Ocean, Deep Sea Drilling Project Hole 548 and 549A. *In* Graciansky, P. C., Poag, C. W., et al., *Init. Repts. DSDP*, 80: Washington (U.S. Govt. Printing Office), 767–792.

________, 1985b. Cenozoic nannofossils, central equatorial Pacific, Deep Sea Drilling Project Leg 85. *In* Mayer, L., Theyer, F., et al., *Init. Repts. DSDP*, 85: Washington (U.S. Govt. Printing Office), 581–607.

Rio, D., Backman, J., and Raffi, I., 1988. *Calcareous Nannofossil Biochronology and the Pliocene/Pleistocene Boundary*: Cambridge (Cambridge Univ. Press).

Roth, P. H., and Thierstein, H., 1972. Calcareous nannoplankton: Leg 14 of the Deep Sea Drilling Project. *In* Hayes, D. E., Pimm, A. C., et al., *Init. Repts. DSDP*, 14: Washington (U.S. Govt. Printing Office), 421–485.

Sager, W. W., 1986. Magnetic-susceptibility measurements of metal contaminants in ODP Leg 101 cores. *In* Austin, J. A., Jr., Schlager, W., et al., *Proc. ODP, Init. Repts.*, 101: College Station, TX (Ocean Drilling Program), 39–45.

Sancetta, C. A., 1983. Biostratigraphic and paleoceanographic events in the eastern equatorial Pacific: results of Deep Sea Drilling Project Leg 69. *In* Cann, J. R., Langseth, M. G., Honnorez, J., Von Herzen, R. P., White, S. M., et al., *Init. Repts. DSDP*, 69: Washington (U.S. Govt. Printing Office), 331–342.

Sanfilippo, A., Westberg-Smith, M. J., and Riedel, W. R., 1985. Cenozoic radiolaria. *In* Bolli, H. M., Saunders, J. B., and Perch-Nielsen, K. (Eds.), *Plankton Stratigraphy*, Cambridge (Cambridge Univ. Press), 631–712.

Schlumberger, Inc., 1972. *The Essentials of Log Interpretation Practice*.

Schrader, H.-J., 1973. Cenozoic diatoms from the northeast Pacific, Leg 18. *In* Kulm, L. D., von Huene, R., et al., *Init. Repts. DSDP*, 18: Washington (U.S. Govt. Printing Office), 673–797.

________, 1974. Cenozoic marine planktonic diatom stratigraphy of the tropical Indian Ocean. *In* Fisher, R. L., Bunce, E. T., et al., *Init. Repts. DSDP*, 24: Washington (U.S. Govt. Printing Office), 887–967.

Schrader, H. J., and Gersonde, R., 1978. Diatoms and silicoflagellates. *Utrecht Micropaleontol.* 17:129–176.

Schultheiss, P. J., 1985. Physical and geotechnical properties of sediments from the Northwest Pacific: Deep Sea Drilling Project Leg 86. *In* Heath, G. R., Burckle, L. H., et al., *Init. Repts. DSDP*, 86: Washington (U.S. Govt. Printing Office), 701–722.

Schultheiss, P. J., Mienert, J., and Shipboard Scientific Party, 1988. Whole-core *P*-wave velocity and gamma ray attenuation logs from Leg 108 (Sites 657 through 668). *In* Ruddiman, W., Sarnthein, M., et al., *Proc. ODP, Init. Repts.*, 108: College Station, TX (Ocean Drilling Program), 1015–1046.

Serra, O., 1984. *Fundamentals of Well Log Interpretation*: Amsterdam (Elsevier).

Shipboard Scientific Party, 1988. Introduction and explanatory notes. *In* Ruddiman, W., Sarnthein, M., et al., *Proc. ODP, Init. Repts.*, 108: College Station, TX (Ocean Drilling Program), 5–28.

Strickland, J.D.H., and Parsons, T. T., 1968. A manual for seawater analysis. *Bull. Fish. Res. Board Can.*, 167:311.

Takayama, T., and Sato, T., 1987. Coccolith biostratigraphy of the North Atlantic Ocean, Deep Sea Drilling Project Leg 94. *In* Ruddiman, W. F., Kidd, R. B., et al., *Init. Repts. DSDP*, 94, Pt. 2: Washington (U.S. Govt. Printing Office), 651–702.

Thierstein, H. R., Geitzenauer, K. R., Molfino, B., and Shackleton, N. J., 1977. Global synchroneity of late Quaternary coccolith datum levels: validation by oxygen isotopes. *Geology*, 5:400–404.

Vincent, E., 1977. Indian Ocean Neogene planktonic foraminiferal biostratigraphy and its paleoceanographic implications. *In* Heirtzler, J. R., et al. (Eds.), *Indian Ocean Geology and Biostratigraphy*: Washington (American Geophysical Union), 469–584.

Von Herzen, R. P., and Maxwell, A. E., 1959. The measurement of thermal conductivity of deep-sea sediments by a needle probe method. *J. Geophys. Res.*, 64:1557–1563.

Wentworth, C. K., 1922. A scale of grade and class terms of clastic sediments. *J. Geol.*, 30:377–390.

Wentworth, C. K., and Williams, H., 1932. The classification and terminology of the pyroclastic rocks. *Bull. Nat. Res. Counc. U.S., Rep. Comm. Sediment.*, 89:10–53.

Zijderveld, J.D.A., Zachariasse, J. W., Verhallen, J.J.M., and Hilgen, F. J., 1986. The age of the Miocene-Pliocene boundary. *Newsl. Stratigr.*, 16:169–181.

Ms 115A-103